

Manuscript Number: RENE-D-20-02028R2

Title: Energy and Exergy analysis of SiO₂/Ag-CuO plasmonic nanofluid on direct absorption parabolic solar collector

Article Type: Research Paper

Keywords: Volumetric absorption parabolic solar collector; Binary nanofluid; Thermal efficiency; Entropy generation.

Corresponding Author: Dr. Shijo Thomas, Ph.D

Corresponding Author's Institution: National Institute of Technology, Calicut

First Author: Albin Joseph, M Tech

Order of Authors: Albin Joseph, M Tech; Sreehari Sreekumar, M Tech; Shijo Thomas, Ph.D

Abstract: Experimental investigations on the application of SiO₂/Ag-CuO plasmonic nanofluid on direct/volumetric absorption parabolic solar collectors is presented in this article. The process variables for the preparation of nanofluid were optimised by employing the desirability function and response surface methodology (RSM). The optimisation was performed to achieve nanofluid with maximum possible thermal conductivity and solar absorptivity. The final solar radiation absorbed fraction and relative thermal conductivity noted for the optimised nanofluid was 82.84% and 1.234, respectively. The performance of the collector was evaluated at various flow rates from 60 lph to 90 lph, using water and optimised nanofluid as the heat transfer fluid. It is noted from the results that the thermal efficiency of the collector increases with the flow rate whereas, the exergy efficiency decreases for both water and nanofluid. The highest temperature difference of 11.27K was noted at 60lph for nanofluid which corresponds to a thermal efficiency of 57.47%. A maximum thermal efficiency of 64.05% was noted at 90 lph which corresponds to an enhancement of 48.19 % in comparison with water. Exergy efficiency of the nanofluid was enhanced by 9.4% at 60 lph, in comparison with water.

Research Data Related to this Submission

There are no linked research data sets for this submission. The following reason is given:

Data will be made available on request

Energy and Exergy analysis of SiO₂/Ag-CuO binary nanofluid on direct absorption parabolic solar collector

Albin Joseph^a, Sreehari Sreekumar^b, Shijo Thomas^{a*}

^a School of Materials Science and Engineering, National Institute of Technology, Calicut 673601, India

^b Department of Mechanical Engineering, National Institute of Technology, Calicut 673601, India

Corresponding author:

Shijo Thomas

School of materials science and engineering

National institute of technology Calicut.

Email address: shijo@nitc.ac.in

Word count: 6072

From

Dr. Shijo Thomas

Assistant professor

School of Materials Science and Engineering

National Institute of Technology, Calicut, India

To

Editor in chief

Renewable Energy

Subject: Submission of revised manuscript for consideration towards publication.

Manuscript Number: RENE-D-20-02028R1

Respected Sir

I thank you for the valuable comments from reviewer. The manuscript has been revised as suggested. The revised **manuscript and response to the reviewers** have been uploaded for favourable consideration.

Thanking you

Yours Sincerely,

Dr. Shijo Thomas

Date: 26/09/2020

Place: NIT Calicut

Reviewer #1 (revision highlighted in yellow)

a. I have one question with regard to uncertainty calculation for the thermal, energy and exergy efficiency. I would request authors kindly give a detailed calculation for the same as response to my question.

The authors noticed a calculation and typographical error in the uncertainty section. We apologise for the same and are thankful to the reviewer for correcting us. The manuscript has been revised and have been rectified. Table 2 presents the revised uncertainties. The revision could be found in page no 10 line no 227-233.

Detailed calculation of uncertainty are presented.

1. Heat gained or useful heat produced (W):

Governing equation: $Q_u = m \cdot Cp \cdot (T_{out} - T_{in})$ (Equation no 3 in the manuscript)

Uncertainty of Eq 3 is given by

$$\frac{\sigma Q_u}{Q_u} = \sqrt{\left(\frac{\sigma m}{m}\right)^2 + \left(\frac{\sigma T_{in}}{T_{in}}\right)^2 + \left(\frac{\sigma T_{out}}{T_{out}}\right)^2}$$

where

$$\sigma m = 0.000625 \frac{kg}{sec}, \quad \sigma T_{in}, \sigma T_{out} = 0.1^\circ C, \quad Q_u = 883.05W, \quad m = 0.025 \frac{kg}{sec}, \quad T_{in} = 30^\circ C,$$

$$T_{in} = 38.41^\circ C,$$

Hence

$$\frac{\sigma Q_u}{Q_u} = \sqrt{(0.025)^2 + (0.0033)^2 + (0.0026)^2} = \pm 2.53\%$$

2. Thermal efficiency

Governing equation: $\eta_{th} = m \cdot Cp \cdot (T_{out} - T_{in}) / (A \cdot I)$ (Equation no 6 in the manuscript)

Uncertainty of Eq 6 is given by

$$\frac{\sigma \eta_{th}}{\eta_{th}} = \sqrt{\left(\frac{\sigma m}{m}\right)^2 + \left(\frac{\sigma T_{in}}{T_{in}}\right)^2 + \left(\frac{\sigma T_{out}}{T_{out}}\right)^2 + \left(\frac{\sigma I}{I}\right)^2}$$

Where

$$\sigma m = 0.000625 \frac{kg}{sec}, \quad \sigma T_{in}, \sigma T_{out} = 0.1^\circ C, \quad \sigma I = 5 \frac{W}{m^2}, \quad I = 850 \frac{W}{m^2}$$

Hence

$$\frac{\sigma \eta_{th}}{\eta_{th}} = \sqrt{(0.025)^2 + (0.0033)^2 + (0.0026)^2 + (0.0058)^2} = \pm 2.60\%$$

3. Exergy efficiency

Governing equation: $\eta_{Ex} = 1 - \frac{T_{amb} \times S_{gen}}{\left[1 - \frac{T_{amb}}{T_{sun}}\right] Q_s}$ (Equation no 10 in the manuscript)

Uncertainty of Eq 10 is given by

$$\frac{\sigma \eta_{Ex}}{\eta_{Ex}} = \sqrt{\left(\frac{\sigma m}{m}\right)^2 + \left(\frac{\sigma T_{in}}{T_{in}}\right)^2 + \left(\frac{\sigma T_{out}}{T_{out}}\right)^2 + \left(\frac{\sigma T_{amb}}{T_{amb}}\right)^2 + \left(\frac{\sigma I}{I}\right)^2}$$

Where

$$\sigma m = 0.000625 \frac{kg}{sec}, \quad \sigma T_{in}, \sigma T_{out}, \sigma T_{amb} = 0.1^\circ C, \quad \sigma I = 5 \frac{W}{m^2}, \quad \sigma T_{amb} = 32^\circ C,$$

Hence

$$\frac{\sigma \eta_{Ex}}{\eta_{Ex}} = \sqrt{(0.025)^2 + (0.0033)^2 + (0.0026)^2 + (0.0031)^2 + (0.0058)^2} = \pm 2.62\%$$

Table. 2: Uncertainties of variables

Variables	Uncertainty
Flow rate	$\leq \pm 2.5 \%$
Solar irradiance	$\leq \pm 5.00 \text{ W/m}^2$
Heat Gained	$\leq \pm 2.53 \%$
Thermal efficiency	$\leq \pm 2.6 \%$
Exergy efficiency	$\leq \pm 2.62 \%$

b. I hope the parabolic concentrator will heat the fluid at-least to a temperature >100 degree celsius. Why authors presented the variation in thermal conductivity only in a low temperature range?

We agree with the reviewers comment. However in the present study the maximum temperature achieved was nearly 50°C. Due to this reason the variation in thermal conductivity was analysed till 50°C.

Highlights

- Influence of $\text{SiO}_2/\text{Ag-CuO}$ nanofluid on direct absorption parabolic collector.
- Exergy and energy analysis was performed at various flow rate
- A maximum thermal efficiency of 64.12 % was noted at 90 lph.
- Exergy efficiency decreased with flow rate whereas thermal efficiency increased.

1 **Energy and Exergy analysis of SiO₂/Ag-CuO plasmonic nanofluid on direct absorption**
2 **parabolic solar collector**

3 Albin Joseph^a, Sreehari Sreekumar^b, Shijo Thomas^{a*}

4 ^a School of Materials Science and Engineering, National Institute of Technology, Calicut
5 673601, India

6 ^b Department of Mechanical Engineering, National Institute of Technology, Calicut 673601,
7 India

8 Corresponding Author: Shijo Thomas, Email Address: shijo@nitc.ac.in

9 **ABSTRACT**

10 Experimental investigations on the application of SiO₂/Ag-CuO plasmonic nanofluid
11 on direct/volumetric absorption parabolic solar collectors is presented in this article. The
12 process variables for the preparation of nanofluid were optimised by employing the
13 desirability function and response surface methodology (RSM). The optimisation was
14 performed to achieve nanofluid with maximum possible thermal conductivity and solar
15 absorptivity. The final solar radiation absorbed fraction and relative thermal conductivity
16 noted for the optimised nanofluid was 82.84% and 1.234, respectively. The performance of
17 the collector was evaluated at various flow rates from 60 lph to 90 lph, using water and
18 optimised nanofluid as the heat transfer fluid. It is noted from the results that the thermal
19 efficiency of the collector increases with the flow rate whereas, the exergy efficiency
20 decreases for both water and nanofluid. The highest temperature difference of 11.27K was
21 noted at 60lph for nanofluid which corresponds to a thermal efficiency of 57.47%. A
22 maximum thermal efficiency of 64.05% was noted at 90 lph which corresponds to an
23 enhancement of 48.19 % in comparison with water. Exergy efficiency of the nanofluid was
24 enhanced by 9.4% at 60 lph, in comparison with water.

25

26 **Keywords:** Volumetric absorption parabolic solar collector, Binary nanofluid, Response
27 surface methodology, Thermal efficiency, Entropy generation.

28

29

30 **Nomenclature**

A	Area of parabola (m^2)	T_{in}	Inlet temperature (K)
A_p	Aperture width of parabola(m)	T_{sun}	Temperature of Sun (K)
C_p	Specific heat of working fluid (kJ/kg.K)	θ	Rim angle of the parabola
E_{des}	Energy destruction (W)	σ	Uncertainty
f	Focal length of the parabola (m)	τ_t	Transmittance of absorber tube
I	Solar irradiance (W/m^2)	r_r	Reflectivity of reflector
m	mass flow rate (kg/sec)	η_{ex}	Exergy efficiency
Q_u	Heat gained (W)	η_{th}	Thermal efficiency
Q_s	Available direct solar energy (W)	η_{opt}	Optical efficiency of the parabola
Q_o	Energy loss (W)	RSM	Response surface methodology
S_{gen}	Entropy generation (W/K)	RTC	Relative thermal conductivity
T_{amb}	Ambient temperature (K)	SRAF	Solar radiation absorbed fraction
		S1	Entropy generated during the transfer of heat to working fluid from solar irradiance
T_{out}	Outlet temperature (K)	S2	Entropy generated during the heat loss

31

32 **1. Introduction**

33 The persistent consumption of fossil fuels made them insufficient to meet the
 34 overwhelmingly increasing demand of energy. Stepping up the utilisation of sustainable
 35 energy sources is a widely acknowledged optimistic solution to meet the ever augmenting
 36 need for energy. Solar energy, a potential replacement to fossil fuels, provides high hope to
 37 overcome the energy crisis to a certain extent, especially in electricity generation and various
 38 heating application [1]. Solar energy being a sustainable and clean source of energy is
 39 gaining widespread attention for many thermal applications. A number of studies have been
 40 reported based on the solar energy conversions like solar thermal conversion, photo electric
 41 conversion and photo electric thermal conversion. The solar thermal convertors like dish
 42 collector, linear Fresnel reflectors (LFR) and parabolic trough collector (PTC) are the most
 43 preferred techniques for the medium and high temperature applications. In these techniques
 44 solar radiation is concentrated to a line or a point from which it is transferred to the working
 45 fluid (heat transfer fluid). Parabolic collectors are widely used for solar thermal application
 46 due to its better performance and comparative cost effectiveness. A parabolic trough
 47 collector is equipped with three components mainly, the parabolic reflector plate equipped
 48 with an absorber tube at its focal point and the working fluid inside the absorber tube. In a

49 typical operation of parabolic collector, solar ray is concentrated (using a parabolic reflector)
50 towards the receiver tube placed at the focal line of the reflector, from which the converted
51 energy in the form of heat is transferred by a working fluid for various applications like water
52 heating, space heating, solar refrigeration system and even for power generation [2]. The
53 solar thermal collectors could be coupled with various thermal systems like power generators,
54 in order to improve the efficiency of the whole unit. Bakos and Tsehelidou [3] investigated
55 solar trough collector coupled with the lignite fired steam power plant using a TRNSYS
56 simulation software. They found that the Rankine efficiency of the plant improved from 33%
57 to 37.64%. They also claim that the solar power plant could reduce the total fuel consumption
58 and thus the CO₂ emission.

59 Apart from the design parameters of the parabolic collector, researchers now a
60 days are focusing on the modification of absorber tubes. Solar absorptivity of the absorber
61 tube is an important parameter that influences the performance of the collector [4, 23]. The
62 absorber tube is an intermediate between the solar radiation and the working fluid. The
63 absorption of solar energy will heat up the absorber tube. This heat is then conducted from
64 the outer surface to the inner surface of the absorber tube which then is transferred to the heat
65 transfer fluid/working fluid through convection. The intermediate heat losses through
66 convection and radiation from the hot absorber tube surface to ambient, results in a
67 deterioration in the performance of the collector [5, 22, 24]. This is where the concept of
68 direct/volumetric absorption solar collectors gains significance by significantly reducing the
69 thermal losses since the photo thermal conversion is directly achieved by the heat transfer
70 fluid/working fluid [6]. Solar radiation absorption capability of the working fluid is the metric
71 of performance of the volumetric absorption solar thermal conversion systems. The poor
72 solar absorptivity of commonly used working fluids like deionised water, ethylene glycol,
73 thermal oils, etc. renders them unfit for direct application in direct absorption collectors.
74 Improving the solar absorptivity of these fluids is an area of active research [7, 8].

75 Nanofluids, with enhanced optical properties, are a suitable replacement for
76 conventional heat transfer fluid in volumetric absorption solar collectors. Qin, et al. [9] made a
77 performance evaluation of novel volumetric solar absorption parabolic collector using
78 plasmonic nanofluids with constant absorption coefficient. An additional reflective coating
79 was given on the upper half of the receiver tube that enhances the optical path length and
80 investigations were performed by varying the receiver tube diameter. They concluded that
81 thermal efficiency of the collector reduced with the diameter and at optimal diameter the
82 direct absorption collector exhibit better performance than the conventional collectors. The

83 authors also claim that direct absorption parabolic collectors are effective at low flowrate
84 (≤ 0.18 kg/s). As per the reports of Bhalla et al. [10] a layer of silicon envelope over the
85 nanofluids could reduce the thermal losses due to convection to the atmosphere. The
86 enhancement on temperature was nearly 3.5°C . Wang et al. [11] introduced a novel technique
87 which improved the efficiency of the direct absorption collector by introducing reverse
88 irradiation. As per their observation the temperature within the fluid was almost uniform
89 compared to the directed irradiated system, which establishes the influence of the
90 nanoparticles in the fluid. However, the enhancement in the properties of nanofluid is limited
91 up to a critical concentration, beyond which the properties of the nanofluid drops. The reason
92 is attributed to reduced stability of the nanofluid at higher concentrations due to the
93 agglomeration and sedimentation of the nanoparticles [28]. Recent reports [12] reveals that
94 binary nanofluids exhibits better properties as compared to conventional nanofluids, due to
95 the combined effect of two or more particles [13]. Bhalla at al. [14] investigated the influence
96 of $\text{Al}_2\text{O}_3/\text{Co}_3\text{O}_4$ binary nanofluid on direct solar absorption system and compared it with that
97 of the surface absorption system. The authors noticed 5.4°C rise in the temperature for
98 optimum direct absorption fluid compared to the surface absorption system. The reports of
99 Chen et al. [15] reveals that improved optical properties are noted for binary nanofluid in
100 which a broad absorption of solar radiation was observed. Zeng and Xuan [16] reports that
101 the plasmonic effect of noble nanoparticles exhibits high photo thermal conversion. SiO_2/Ag
102 is one of the commonly used plasmonic nanoparticles. However, the hybrid nanoparticles are
103 found to be larger in size due to which the stability of the nanofluid is affected highly. As per
104 the reports of Keblinski et al. [17] the particles size have very high impact on stability and
105 properties of the nanofluid. The improved effectiveness of the nanofluid is observed at lower
106 particle size. Thermo-optical properties of the nanofluid have very high significance in the
107 direct absorption solar collector [29, 30]. Due to this reason it is highly recommended to
108 employ working fluid with high thermal and optical properties in volumetric absorption solar
109 collectors. From these perspectives, it is clear that the binary nanofluid in which more than
110 one nanoparticles are dispersed, is capable to achieve both. The colloidal stability of the
111 nanoparticles in the fluid is one of the main practical drawback associated with nanofluids.
112 Nevertheless, this issue can be addressed by various methods like addition of surfactants,
113 varying pH of the fluid, surface functionalization of the nanoparticles, etc. By enhancing the
114 mutual repulsion between the particles, the chance of agglomeration of the particles and
115 further sedimentation can be prevented. Zeta potential analysis is one of the method used to
116 quantify the colloidal stability of nanofluids. An absolute value of zeta potential greater the

117 30 mv is considered to yield a stable nanofluid. However, for flow applications the issue of
118 the stability is less pronounced since the fluid under circulation is in continuous agitation
119 [18].

120 In the present study the performance evaluation of the volumetric absorption collector
121 using plasmonic SiO₂/Ag-CuO binary nanofluid is investigated experimentally. Additional
122 advantages on photo-thermal conversion of nanofluid could be observed in SiO₂/Ag particles
123 due to the plasmonic effect, the thermal transport within the nanofluid is being influenced by
124 the CuO nanoparticles. The desirability function combined with the response surface
125 methodology (RSM), a widely adopted technique in industries for multi objective response
126 process, was used to optimise the process variables involved in the study [19, 20]. The
127 experiments were conducted at National Institute of Technology Calicut (latitude: 11.3216,
128 longitude: 75.9336). Thermo-optical properties exhibited by the nanofluid as well as the
129 collector efficiency and entropy generation of the collector are analysed using the optimised
130 SiO₂/Ag-CuO nanofluid, and compared with base fluid. Even though many lab scale studies
131 on the optical properties of plasmonic nanofluid were reported, to the best of the author's
132 knowledge this is the first attempt that investigates the influence of a plasmonic binary
133 nanofluid on a volumetric absorption parabolic collector.

134 **2. Materials and methods**

135 *2.1 Synthesis of SiO₂/Ag-CuO nanofluid.*

136 SiO₂/Ag-CuO nanofluid was synthesised by two step method in which the particles
137 are added and dispersed in the water. SiO₂/Ag particle used in the fluid was prepared by
138 introducing Ag on the SiO₂ by reducing AgNO₃ with SnCl₂. CuO nanoparticles used are
139 directly purchased from Sigma Aldrich. To achieve a stable suspension, sodium dodecyl
140 sulfonate was used as surfactant. Optimisation of the concentration of nanoparticle and
141 surfactant were done using a desirability function. The detailed procedure of synthesis of
142 nanofluid and optimisation is mentioned in the earlier investigation conducted by the same
143 authors [28]. The optimised nanofluid is then used in the volumetric absorption solar
144 collector.

145 *2.2. Design and manufacturing of experimental setup.*

146 *2.2.1 Parabolic reflector*

147 The length of parabolic trough is 1500 mm and the aperture width is 1080 mm. Three
 148 troughs of dimensions 500 mm length and 1080mm aperture diameter each were fabricated
 149 using the glass wool - epoxy composite. Anodised aluminium sheets were used as the
 150 reflector. The reflector sheets were fixed on the glass wool-epoxy composite parabolic trough
 151 so that the reflector attain the parabolic trough shape. The rim angle of the parabola is 90° and
 152 Eq. 1 represents the parabolic profile of the fabricated trough.

$$153 \quad Y = 0.925X^2 \quad (1)$$

154 The focal point of the parabola is given by equation 2

$$155 \quad f = \frac{Ap}{2} \cot\theta + \frac{Ap^2}{16f} \quad (2)$$

156 Where f is focal length of the parabola, θ is the rim angle and A_p , the aperture width of the
 157 parabola.

158 The dimensions of the parabolic trough are presented in Table 1.

159 **Table. 1: Dimension of parabolic trough fabricated.**

Parameter	Dimension
Length of parabola	1.5 m
Distance of focal point	0.272 m
Aperture width	1.05m
Aperture Area	1.575 m ²
Rim angle	90°
Outer tube inner diameter	0.035 m
Inner tube inner diameter	0.015 m

160

161 2.2.2 Absorber Tube.

162 Optical absorptivity and other dimensions of the absorber tube highly influences the
 163 thermal and optical efficiency of a parabolic solar collector. In the present system, glass-glass
 164 absorber tube made of quartz is used, which enable high transmittance, reducing the optical
 165 losses of absorber tube. Moreover, the evacuation of glass- glass annulus could reduce the
 166 convective heat losses [10]. A provision was made on the experimental setup to adjust the
 167 position of the absorber tube so as to maintain the absorber tube exactly at the focal point of

168 the parabolic trough. Both ends of the absorber tube were sealed using Teflon coupling which
169 could withstand temperature up to 350°C and high temperature RTV silicon (anabond) was
170 used as sealant.

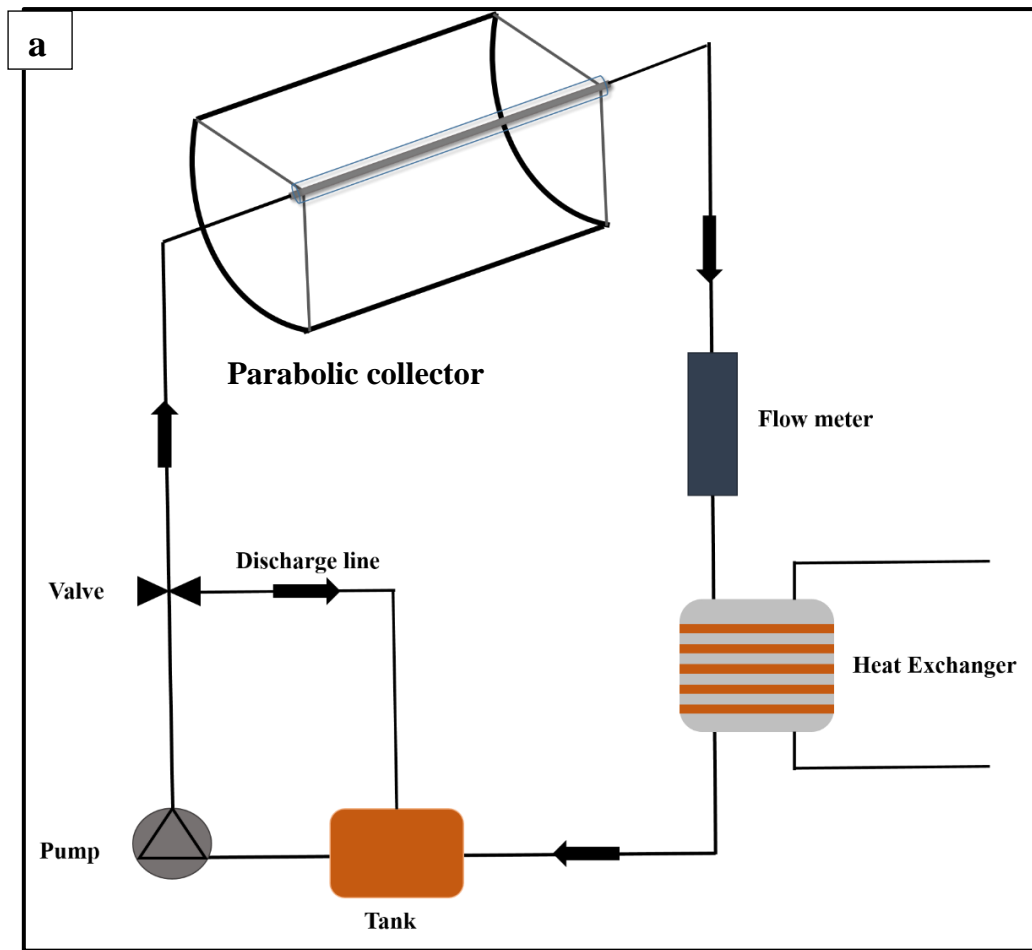
171 *2.2.3 Solar Tracker*

172 Continuous tracking of sun is mandatory for the collector to get perpendicular rays on
173 its surface. To accomplish this a solar tracker was employed. The tracker consist of a geared
174 motor which is connected to the axis of parabolic collector. The sun tracking was achieved
175 using an LDR photo resister as the sensor. The LDR sensor unit (not clear in the figure due to
176 its small size) placed on the trough is connected to geared motor unit with an intermediate
177 PCB circuit.

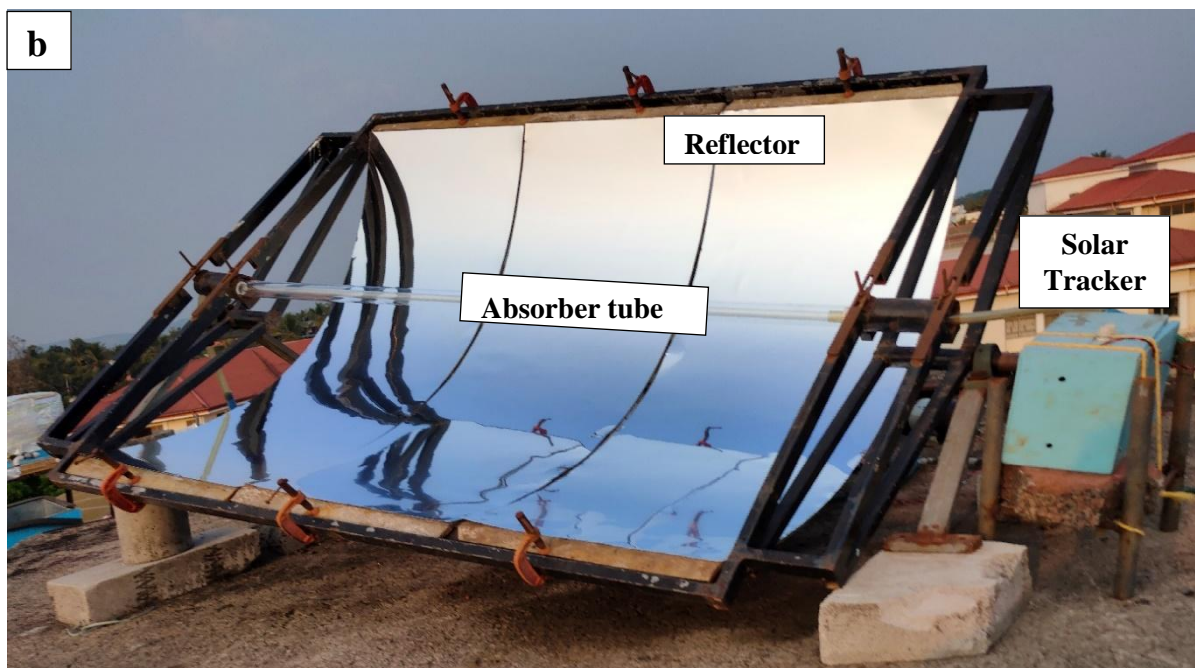
178 *2.2.4 Experimental procedure.*

179 The parabolic trough collector used in the present study is located at National Institute
180 of Technology, Calicut in the North-South direction (latitude: 11.3216, longitude: 75.9336).
181 The experiment was carried out on clear sunny days during the month of March and April.
182 The hydraulic cycle chosen for the study is shown in Fig 1. According to Fig 1 the nanofluid
183 from a reservoir is pumped to the parabolic collector and then to a heat exchanging unit
184 (constant temperature bath). The heat exchanger cools the nanofluid and maintain a constant
185 temperature at the inlet of absorber tube. The nanofluid from the heat exchanger is finally
186 directed to the reservoir. The flow rate of the nanofluid was varied using a valve and flow
187 meter. The inlet and outlet temperatures were noted using calibrated T-type thermocouples,
188 connected to a data logger (Agilent). The temperatures were noted at every 5 minutes interval
189 from 09:45 am to 4:15 pm and average temperature for every 30 minutes were determined.

190 As mentioned in Section 2.2 the nanofluid was synthesised based on the range of
191 concentration mentioned in Table 3 and its thermo-optical properties were measured. An
192 optimised process variables of nanofluids were achieved that enables maximum possible
193 solar radiation absorption and thermal conductivity. The nanofluid prepared using this
194 optimised combination is further experimentally analysed to quantify its effect on volumetric
195 absorption parabolic collector (VAPC). The influence of this nanofluid on VAPC at various
196 flow rates starting from 60 lph to 90 lph, were analysed and compared with that of base fluid.



197



198

199 Fig. 1. a) Schematic of experimental setup, b) Photograph of fabricated parabolic trough

200

201 *2.3 Mathematical formulation*

202 Mathematical formulation used for the estimation of performance parameters are listed
203 below:

204 Useful heat produced (W):

205
$$Q_u = m \cdot Cp \cdot (T_{out} - T_{in}) \quad (3)$$

206 Available direct solar energy:

207
$$Q_s = A \cdot I \quad (4)$$

208 Optical and thermal efficiency of the parabola was calculated using equation 5 and 6

209
$$\eta_{opt} = \tau_t r_r \quad (5)$$

210
$$\eta_{th} = \frac{Q_u}{Q_s} \quad (6)$$

211 Entropy generation (W/K):

212
$$S_{gen} = mCp \ln\left(\frac{T_{out}}{T_{in}}\right) - \frac{Q_s}{T_{sun}} + \frac{Q_o}{T_{amb}} \quad (7)$$

213 The entropy generation during the heat transfer from sun to nanofluid and inside absorber
214 tube was estimated using Eq 7. The entropy generated due to the pressure drop during fluid
215 flow is neglected as it was insignificant.

216
$$Q_o = Q_s - mCp (T_{out} - T_{in}) \quad (8)$$

217 Energy destruction (W):

218
$$E_{des} = S_{gen} \times T_{amb} \quad (9)$$

219 Exergy efficiency:

220
$$\eta_{Ex} = 1 - \frac{T_{amb} \times S_{gen}}{\left[1 - \frac{T_{amb}}{T_{sun}}\right] Q_s} \quad (10)$$

221

222

223 *2.4 Experimental Uncertainty Analysis*

224 The uncertainty experimental data was estimated using the method described by Moffat [26].
 225 Table 2 presents the estimated uncertainty of various parameters. The calibration of
 226 thermocouple was done by employing a constant temperature bath as standard. The
 227 maximum error in the thermocouple was found to be $\pm 0.1\text{K}$, the uncertainty of Heat gained,
 228 thermal and exergy efficiency was calculated from the equation 11-13

$$229 \quad \frac{\sigma Qu}{Qu} = \sqrt{\left(\frac{\sigma m}{m}\right)^2 + \left(\frac{\sigma T_{in}}{T_{in}}\right)^2 + \left(\frac{\sigma T_{out}}{T_{out}}\right)^2} \quad 11$$

$$230 \quad \frac{\sigma \eta_{th}}{\eta_{th}} = \sqrt{\left(\frac{\sigma m}{m}\right)^2 + \left(\frac{\sigma T_{in}}{T_{in}}\right)^2 + \left(\frac{\sigma T_{out}}{T_{out}}\right)^2 + \left(\frac{\sigma I}{I}\right)^2} \quad 12$$

$$231 \quad \frac{\sigma \eta_{Ex}}{\eta_{Ex}} = \sqrt{\left(\frac{\sigma m}{m}\right)^2 + \left(\frac{\sigma T_{in}}{T_{in}}\right)^2 + \left(\frac{\sigma T_{out}}{T_{out}}\right)^2 + \left(\frac{\sigma T_{amb}}{T_{amb}}\right)^2 + \left(\frac{\sigma I}{I}\right)^2} \quad 13$$

232 **Table. 2: Uncertainties of variables**

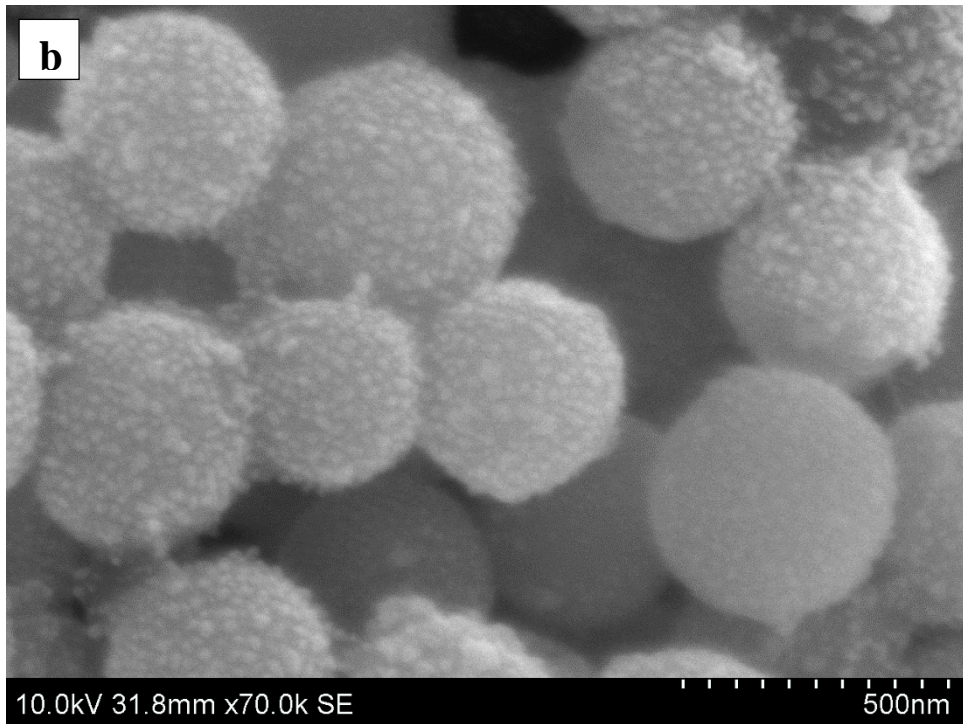
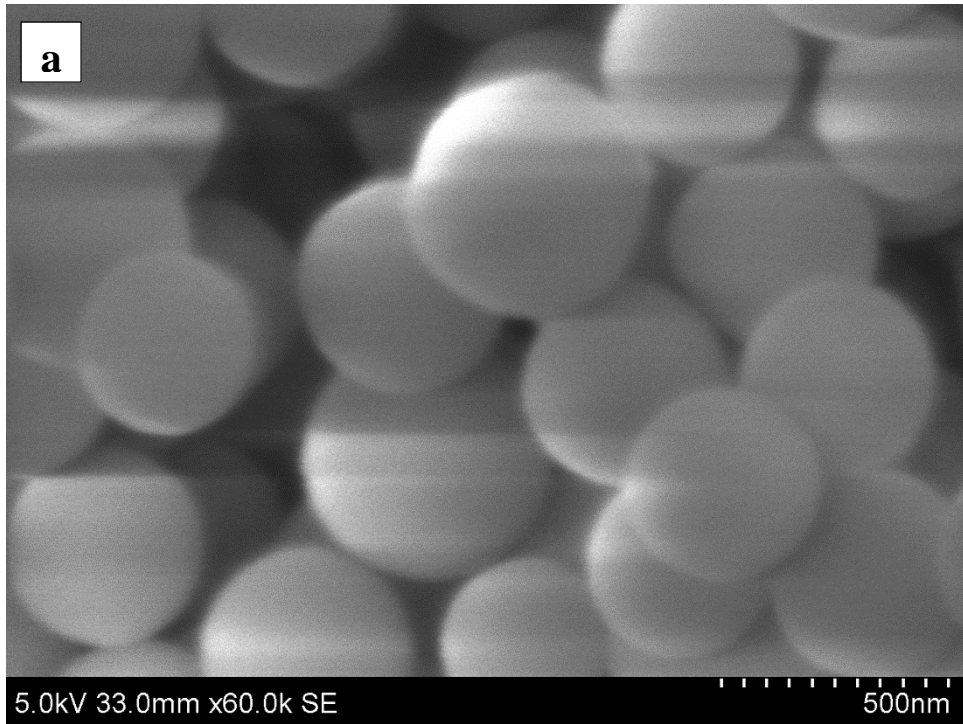
Variables	Uncertainty
Flow rate	$\leq \pm 2.5 \%$
Solar irradiance	$\leq \pm 5.00 \text{ W/m}^2$
Heat Gained	$\leq \pm 2.53 \%$
Thermal efficiency	$\leq \pm 2.6 \%$
Exergy efficiency	$\leq \pm 2.62 \%$

233

234 3. Result and discussion

235 3.1 Characterisation of nanofluids

236 Characterisation was limited to measurement of solar absorptivity and thermal
 237 conductivity of nanofluid and morphological analysis of nanoparticles. Data obtained from
 238 the UV-vis spectrometer (Avantes) was used to estimate the solar radiation absorbed fraction
 239 (SRAF). To quantify the thermal conductivity exhibited by the nanofluids, a thermal
 240 properties analyser (KD2 pro) was employed. Morphology of the nanoparticles were analysed
 241 using the field emission scanning electron microscope (Hitachi SU 6600) and are presented in
 242 Fig 2.



245 **Fig. 2.** SEM images a) SiO₂, b) SiO₂/Ag nanoparticles.

246 *3.2 Optimisation of SiO₂/Ag-CuO plasmonic binary nanofluid*

247 The optimisation of the nanofluid is detailed in the earlier publication by the same
248 authors [28]. Desirability approach on RSM was adopted to optimise the process variables
249 involved in the synthesis of nanofluid. Desirability function is a widely adopted approaches

250 to optimise multi objective problems [20]. The regression equation for relative thermal
 251 conductivity and SRAF obtained from the central composite design of response surface
 252 methodology (Eq. 14 and 15) was taken for the desirability approach [28]. The objective of
 253 the optimisation was to maximise SRAF and thermal conductivity of the nanofluids. In this
 254 approach the variables such as mass of nanoparticles like SiO₂/Ag and CuO, surfactant are in
 255 the design range (between upper limit and lower limit), while the responses like thermal
 256 conductivity and SRAF are set to be maximal. Table 3 presents the goal, lower and upper
 257 limit and importance of each process variables. The optimal combination of process variables
 258 was obtained as 206.3 mg of SiO₂/Ag per litre of DI water and correspondingly, 864.7 and
 259 1996.2 mg of CuO and SDS respectively. Figure 3 shows the variation of desirability with
 260 change in concentration of particles. It can be seen that, the desirability drops after
 261 concentration of SiO₂/Ag particles exceeds 206.3 mg/l, which might be due to the fact that
 262 beyond this concentration the stability of the nanofluid decreases resulting in a decrease in
 263 thermal conductivity and SRAF. However, the desirability increased with the concentration
 264 of CuO and then drops after 864.7mg/l. This could be due to the fact that, as the CuO
 265 concentration increases the thermo-optical properties are found to be increased and after a
 266 critical concentration the stability of the nanofluid was affected, thus decreasing the
 267 desirability. Moreover, the stability was found to be increased with surfactant concentration
 268 due to which the desirability increases with the concentration of surfactant. The optimised
 269 concentrations of nanoparticles were found to be stable with a zeta potential of -38.7mV. The
 270 RTC and SRAF for the optimised concentration were found to be 1.234 and 82.84%
 271 respectively from the response equations. To confirm this experimentally, the optimised
 272 nanofluid combination was prepared and the experimental value of RTC and SRAF were
 273 obtained as 1.231 and 81.79% respectively. Since the predicted and experimental values are
 274 comparable to each other in addition with the desirability value of one, the results are
 275 reliable. The final optimised nanofluid is then taken to the parabolic collector for the analysis
 276 of photo thermal conversion and entropy generation. In addition thermal conductivity of the
 277 optimised nanofluid in the temperature range, 30°C to 50°C, was measured and presented in
 278 the Table 4. The relative thermal conductivity (Thermal conductivity of nanofluid by thermal
 279 conductivity of water) was also estimated.

280 .

281
$$RTC = 1.11825 + (4.64016 \times 10^{-005} \times C) + (8.23773 \times 10^{-006} \times B) - (7.08371 \times 10^{-005} \times A) -$$

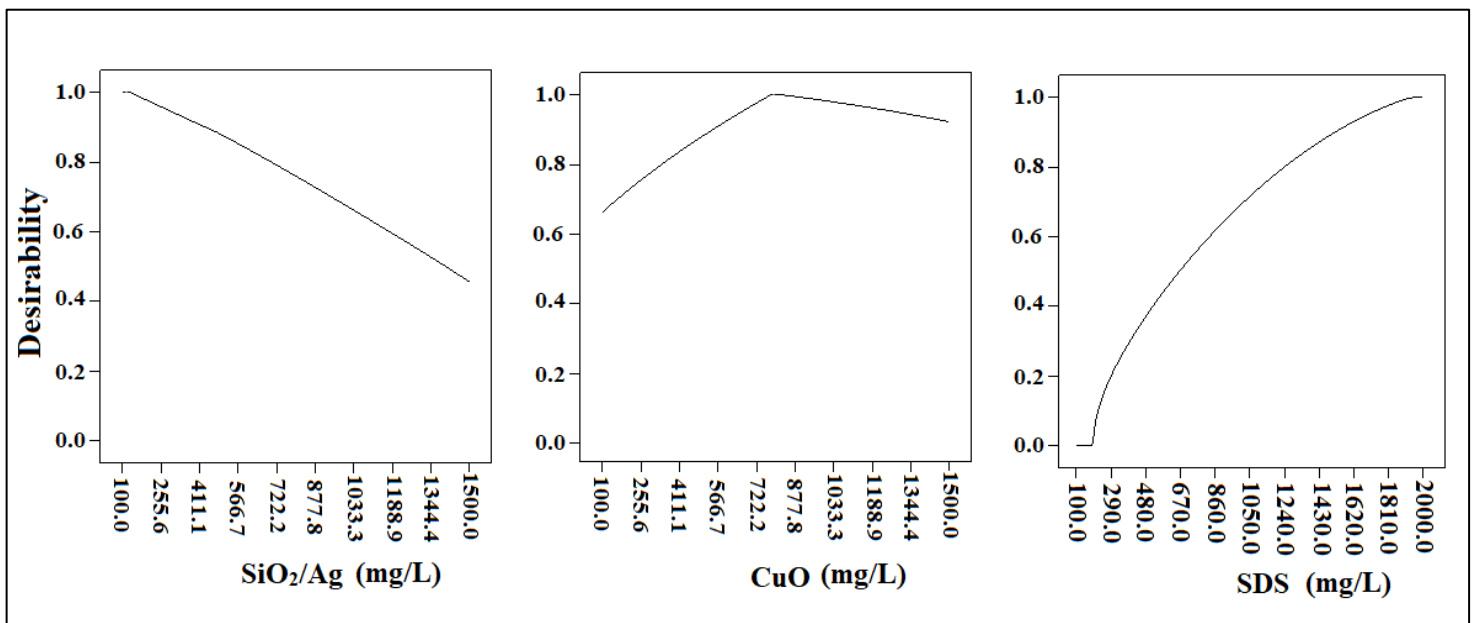
 282
$$(2.81400 \times 10^{-008} \times A \times B) + (7.00727 \times 10^{-008} \times B \times C) - (1.48865 \times 10^{-008} \times A \times C) -$$

283 $(1.87837 \times 10^{-008} \times C^2) - (6.43326 \times 10^{-009} \times B^2) + (3.11178 \times 10^{-008} \times A^2)$
 284 (14)

285 $SRAF = 35.2379 + (0.039759 \times C) + (0.010745 \times B) + (0.021866 \times A) - (3.34793E-006 \times A$
 286 $\times B) - (6.48624 \times 10^{-006} \times B \times C) - (6.67764 \times 10^{-006} \times A \times C) - (7.30303 \times 10^{-006} \times C^2) -$
 287 $(1.95099 \times 10^{-006} \times B^2) - (1.08898 \times 10^{-005} \times A^2)$
 288 (15)

289 Where A, B, and C are mass of SiO₂/Ag, CuO and SDS respectively per litre of DI water.

290



292 **Fig .3.** Variation of desirability function with process variables.

293 **Table. 3:** Conditions adopted during the optimisation.

Name	Goal	Lower limit	Upper limit	Importance
Concentration of SiO ₂ /Ag (mg/l)	In range	100	1500	4
Concentration of CuO (mg/l)	In range	100	1500	4
Concentration of SDS (mg/l)	In range	100	2000	4

294

295

296 **Table 4.** Thermal conductivity at various temperature

Temperature (°C)	Relative thermal conductivity	Thermal conductivity (W/mK)
30	1.234	0.7404
35	1.248	0.7491
40	1.262	0.7576
45	1.299	0.7794
50	1.314	0.7886

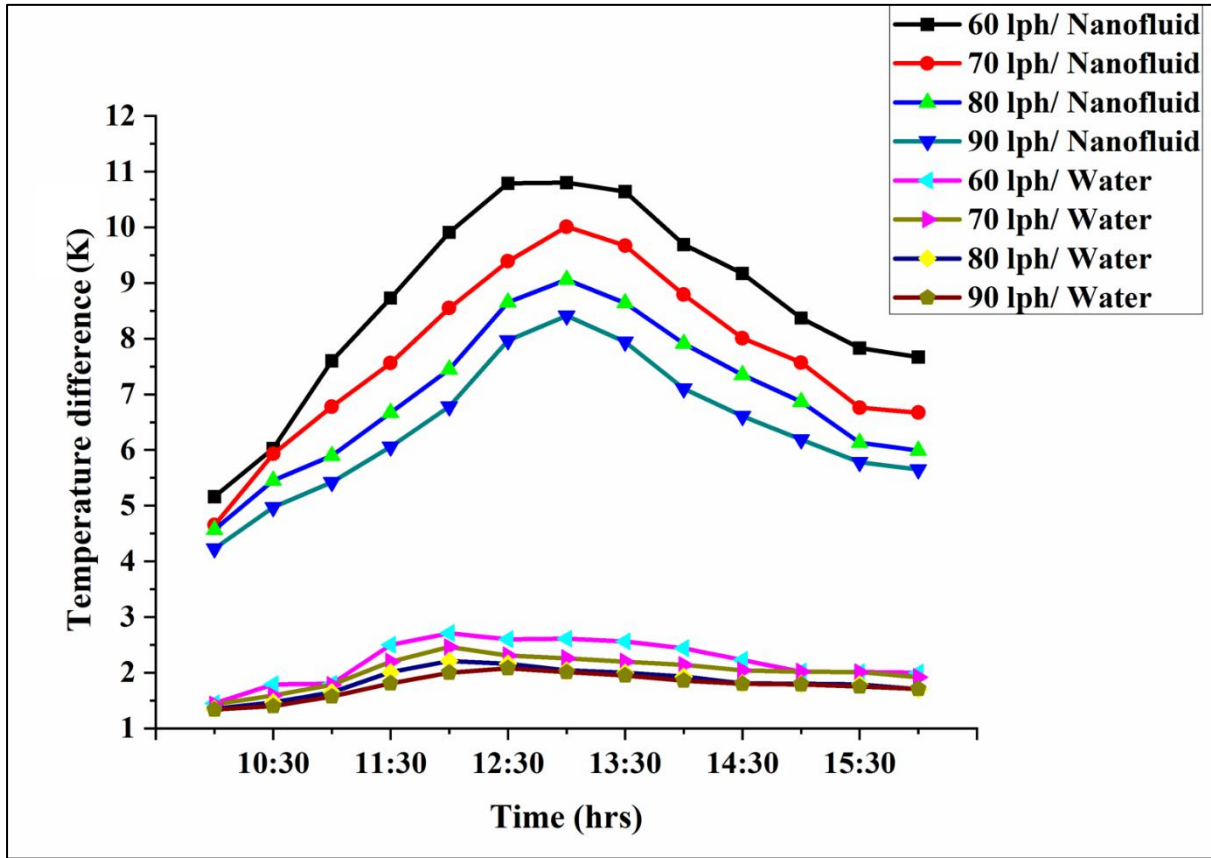
297

298 **3.3 Performance of SiO₂/Ag-CuO hybrid plasmonic nanofluid on parabolic collector.**

299 The SiO₂/Ag-CuO nanofluid used as working fluid in the parabolic collector was
 300 prepared based on the optimum process variables achieved from the procedure mentioned in
 301 3.2. The optimised valued of mass of particles and surfactant (process variables for preparing
 302 the nanofluid) are 206.3 mg/L, 864.7mg/L and 1996.2mg/L of SiO₂/Ag, CuO and SDS
 303 respectively. The experiment was carried out on a sunny day during the month of March and
 304 April. The Average solar radiation in the experimental location was 850 W/m². The
 305 maximum radiation noted was 950W/m² which mostly occur during 12:00 pm to 2:00 pm.

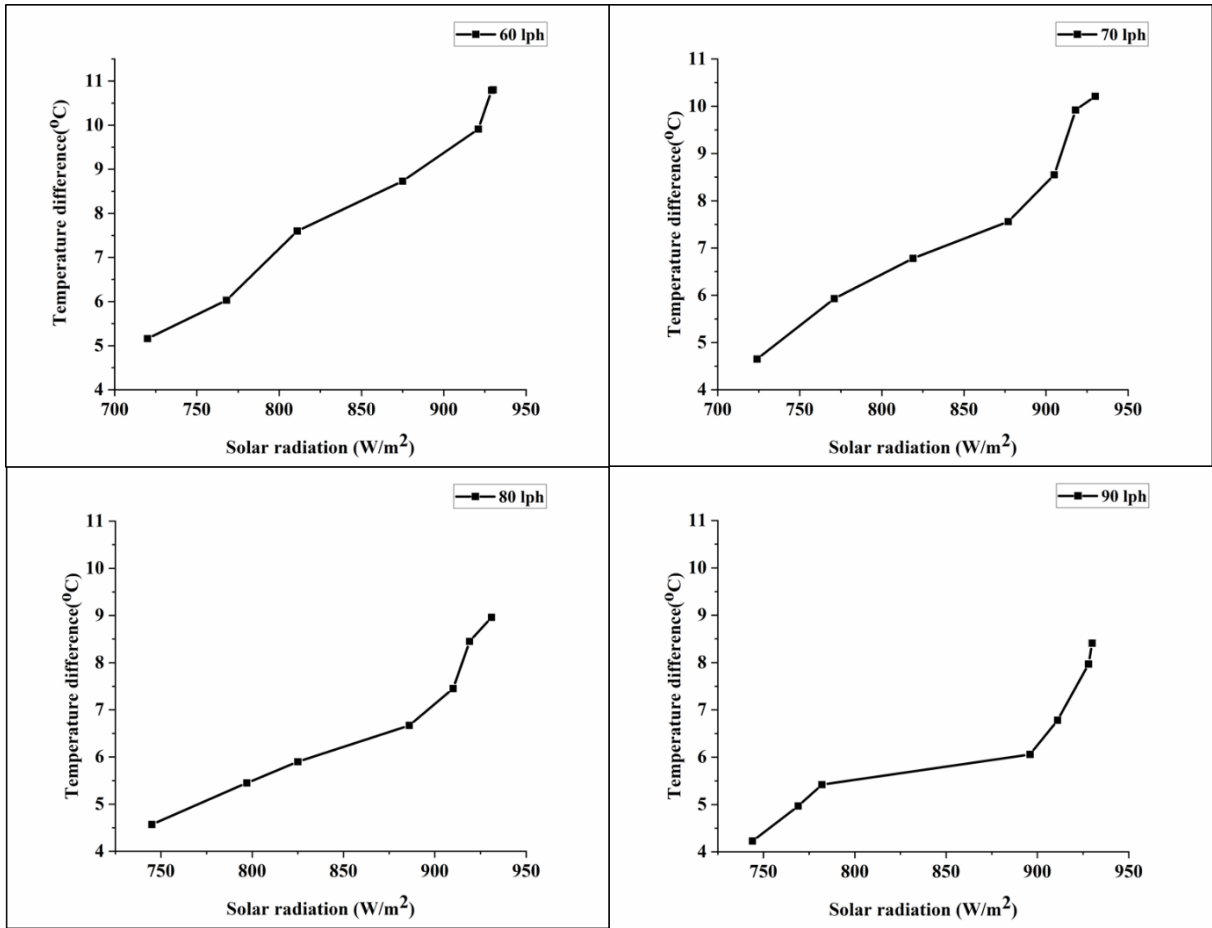
306 Figure 4 presents the temperature profile of nanofluid and the base fluid at various
 307 flow rates. The temperatures were noted from 10:00 am to 4:00 pm. As the figure says the
 308 temperature difference decreases with the increase in flow rate of working fluid. A maximum
 309 temperature difference of 11.27K was noted for the optimum nanofluid at the flow rate of 60
 310 lph and 8.4K at 90 lph. The highest noted temperature difference for water was 2.61K, at
 311 60lph. Table 4 shows the maximum temperature difference obtained for SiO₂/Ag-CuO
 312 nanofluid and water at various flow rates. It is apparent that the introduction of nanoparticles
 313 enhanced the performance of the collector by improving the optical and thermal properties of
 314 the nanofluid. The improved solar absorptivity of the nanofluid increased the solar thermal
 315 conversion of the collector and the enhancement in thermal conductivity augmented the heat
 316 transfer for nanofluids. The experiments were repeated three times and the reported values
 317 are the average, to ensure the repeatability. The variation of temperature difference with solar
 318 radiation is plotted and added in the manuscript as Figure 5. As can be seen form the figure
 319 the temperature difference increases with the solar radiation for a particular flow rate and the
 320 variation is almost linear. At a flow rate of 60 lph, the maximum temperature difference
 321 obtained was 10.8 °C for 930 W/m². The minimum temperature difference observed at this
 322 flow rate was 5.16 °C at a solar radiation of 720 W/m². The maximum temperature noted at
 323 90 lph was 8.41 °C at 930 W/m² for which the maximum efficiency was also obtained. The

324 maximum observed temperatures were 10.21 °C and 8.96 °C at flow rates of 70 and 80 lph
325 respectively for a solar radiation of 930 W/m²



326

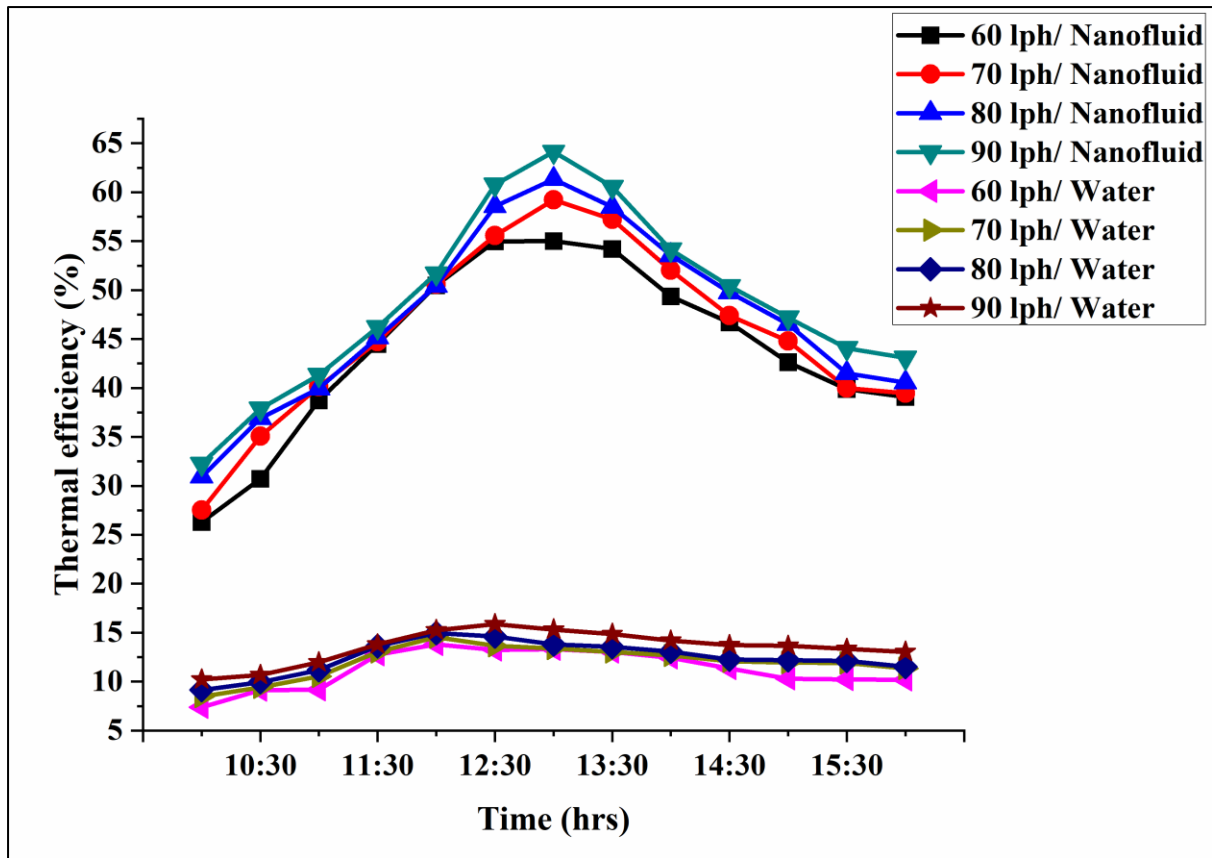
327 **Fig. 4.** Temperature profile of nanofluid and water at various flow rates.



328

329 **Fig. 5** Variation of temperature difference with radiation.

330



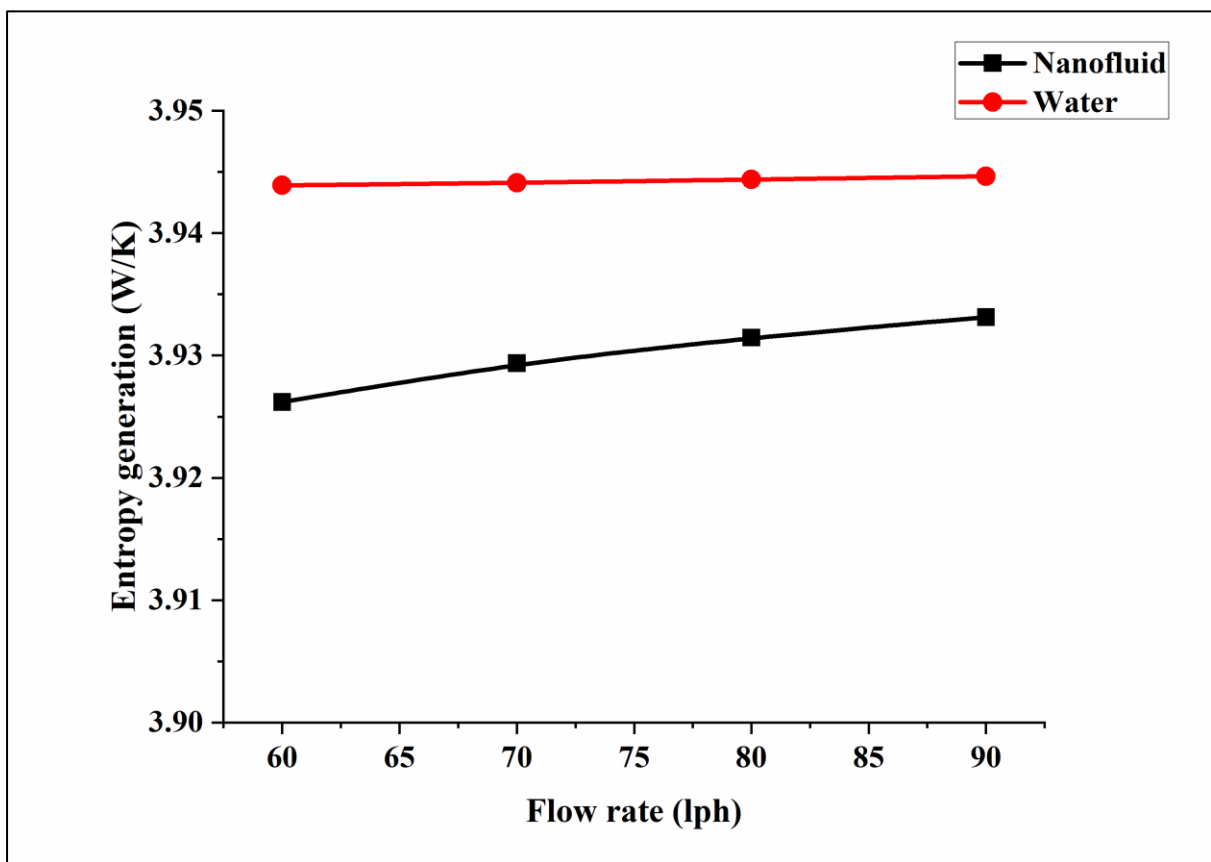
331

332 **Fig. 6.** Thermal efficiency plot of nanofluid and water at various flow rates.

333

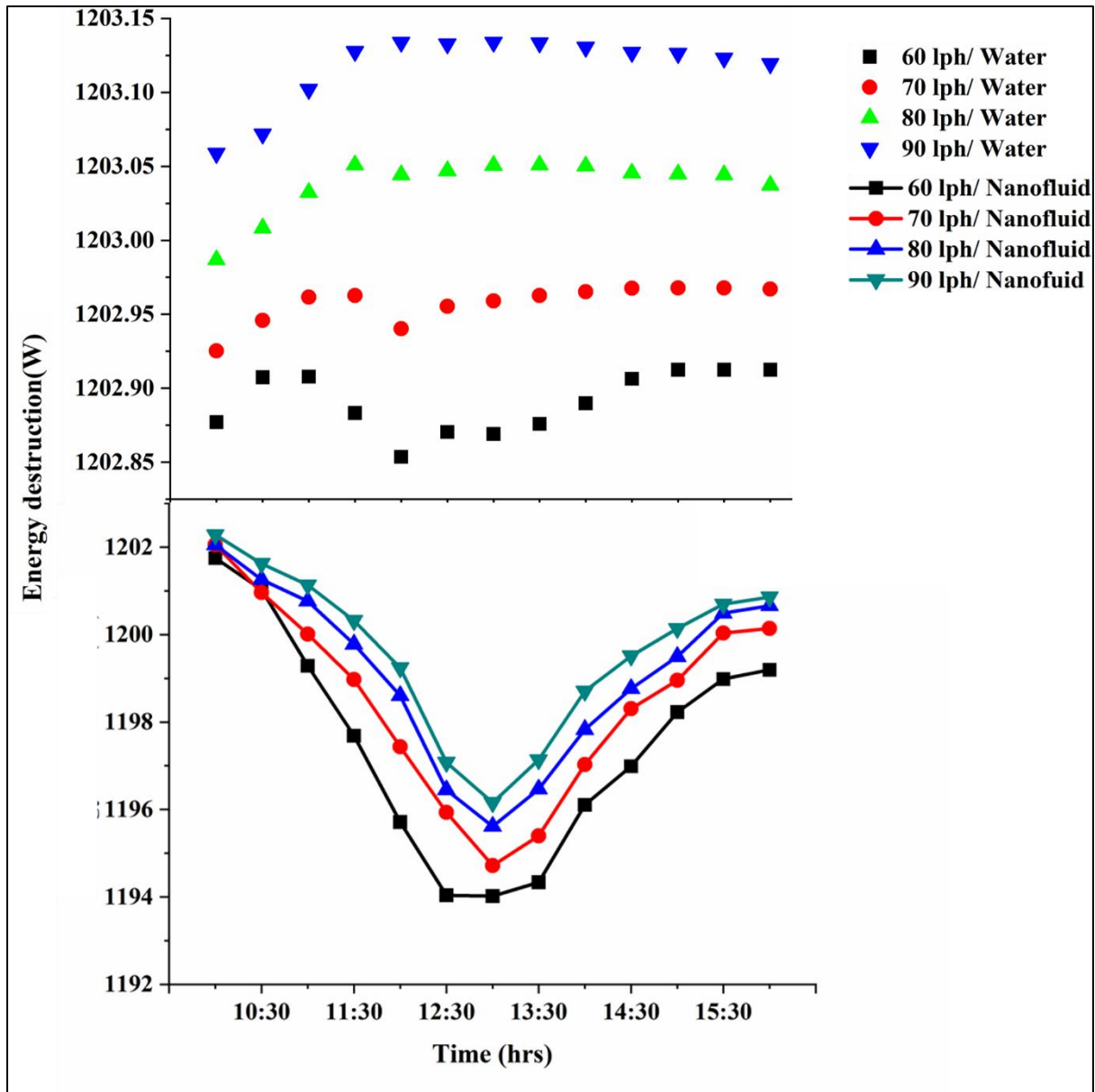
334 The thermal efficiency of the collector was estimated using the equations 3, 4, 5 and
 335 6. The transient variation of collector efficiency at various flow rate are shown in Fig. 6. The
 336 direct solar irradiance is 850 W/m^2 , which is the estimated average solar radiation at the
 337 location. The maximum thermal efficiencies for water are 13.29, 14.55, 14.96 and 15.86% at
 338 flow rates of 60, 70, 80 and 90 lph, respectively. The corresponding values of efficiencies
 339 estimated for nanofluid are 57.40, 60.41, 63.72 and 64.13% respectively. In addition, it could
 340 be observed from Fig. 6 that the maximum efficiency was obtained during the time period of
 341 12:00 pm to 2:00 pm. As mentioned before, the efficiency of the collector depends on the
 342 thermo-optical properties of the working fluid. Plasmonic SiO_2/Ag nanoparticles used in the
 343 present investigation exhibited an additional improvement in the optical absorptivity of the
 344 fluid which in turn resulted in better photo thermal conversion. It is reported that in
 345 comparison with other nanoparticles plasmonic nanoparticles exhibit an additional self-
 346 heating due to the plasmonic effect, which in turn enhance the photo thermal conversion
 347 efficiency of the nanofluid [16, 21]. The presence of CuO in the fluid transfers the absorbed

348 solar energy effectively, which is attributed to its higher thermal conductivity [17]. Reynolds
349 number is another parameter that influences the efficiency of the collector. The heat transfer
350 becomes more effective as the Reynolds number/ flow rate increases which also results in the
351 increased efficiency of the collector [25, 31]. As explained in equation (6) thermal efficiency
352 of the collector is defined as the ratio of useful heat produced to the available direct solar
353 energy. As the flow rate increases the amount of useful heat carried away by the working
354 fluid increases. As the flowrate increases the local mixing between the fluid and solid
355 particles and also between the fluid and the tube surface increases which results in enhanced
356 thermal transport and reduced thermal loss [32].



357

358 **Fig. 7.** Average entropy generation at various flowrates.

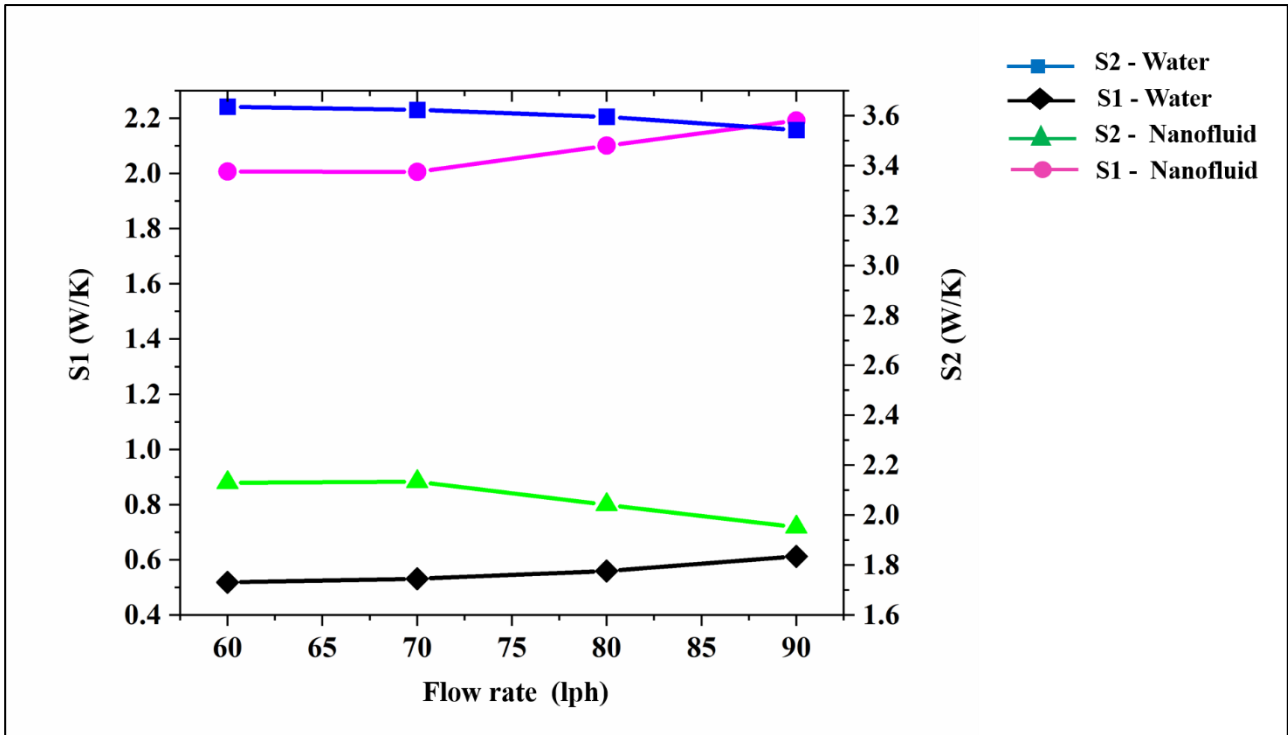


359

360 **Fig. 8.** Energy destruction profile of nanofluid and water at various flowrates.

361 Figures 7 and 8 shows the entropy generation and energy destruction calculated using
 362 equations 7, 8, 9 and 10. As can be seen from Figure 7, the entropy generation slightly
 363 decreased with the dispersion of nanoparticles in water. The entropy generation was almost
 364 constant with change in flow rate in the case of water, while it slightly increased with
 365 flowrate for nanofluid. In the present study, two factors could be accounted for the entropy
 366 generation. 1) Entropy generation due to the heat transfer from solar irradiance to the
 367 nanofluid (S1). 2) Entropy generated during to the heat loss from the nanofluid to the
 368 surroundings (S2). The contribution of the two sources (S1 & S2) to entropy generation in
 369 water and nanofluids at different flow rates is shown in Fig. 9. Among these two sources, the

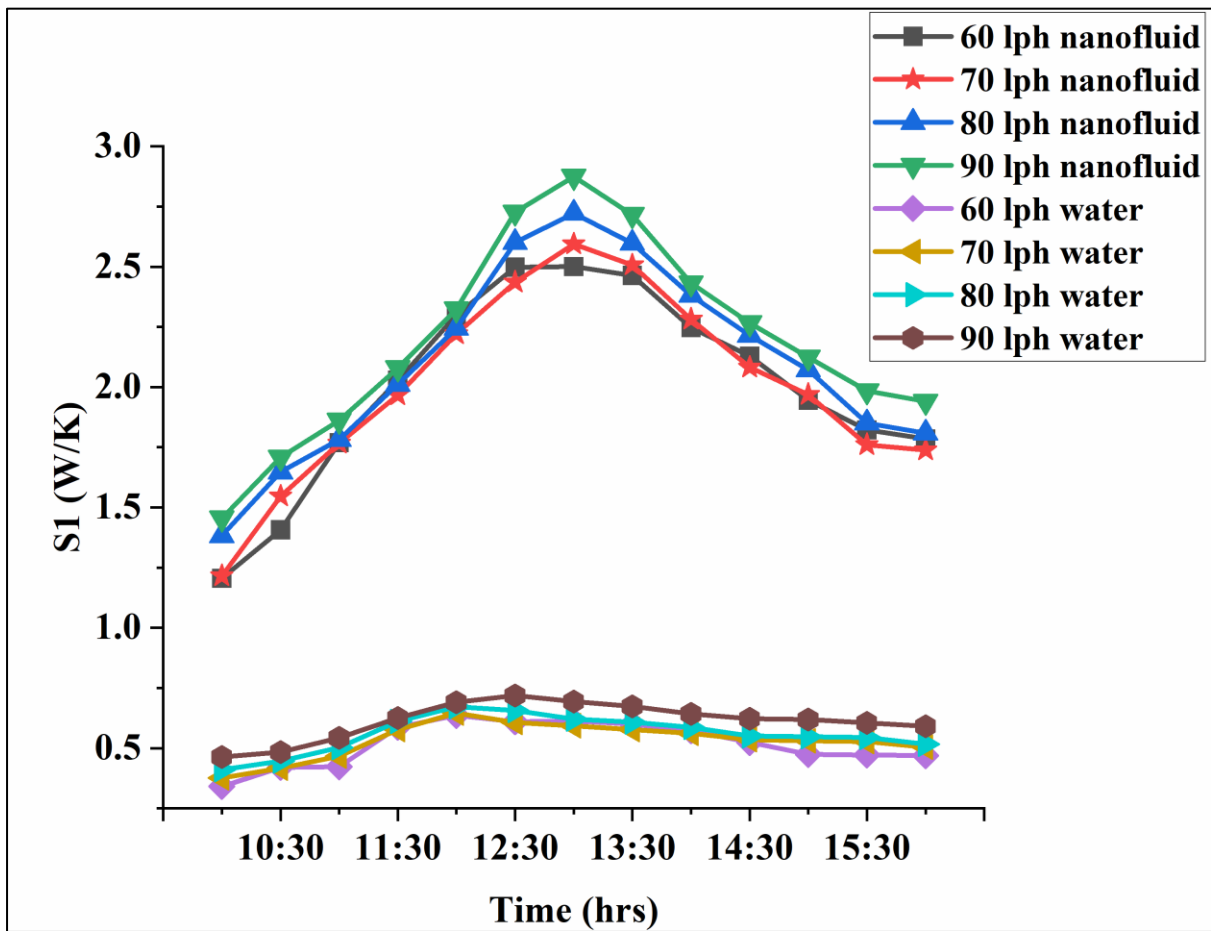
370 entropy generation due to the heating up of the nanofluid as it flows through the collector
371 tube from inlet to outlet (S_1) was found to be lesser than the entropy generation due the heat
372 losses from the nanofluid (S_2). At a flowrate of 90 lph the S_1 for water was 72.14% lower
373 than that of nanofluid. The S_1 for water was found to be less compared to nanofluid since the
374 heat gain was less in water when compared to nanofluid. However, entropy generated due to
375 the losses (S_2) was found to be less compared to water and reduces with the flow rate for
376 nanofluids. At a flowrate of 90 lph the S_2 for water is 81.54% higher than that of nanofluid.
377 The contribution of entropy generation due to heat losses (S_2) of water being much higher
378 than that of nanofluid is the reason for the slight increase in overall entropy generation
379 (S_1+S_2) of water with flow rate. On comparing figures 10 and 11 with Fig. 4 it can be seen
380 that, at a particular flow rate S_1 increases with temperature difference whereas S_2 decreases
381 (Fig 10 and 11). The higher absorption of heat by the plasmonic nanofluids results in higher
382 temperature gain of the fluid and thus contributes to S_1 . In spite of the high temperature rise
383 of the fluid the heat losses to the ambient is lesser in volumetric absorption systems
384 employing plasmonic nanofluids is evident from the decreasing S_2 values. The variation of
385 thermal efficiency and exergy efficiency with the flow rate is presented in Fig 12. It can be
386 seen that in the case of the optimised nanofluid, the exergy efficiency shows a slight decrease
387 with flow rate, while thermal efficiency increases. But the exergy efficiency of the nanofluid
388 was found to be higher than that of water with an enhancement of 9.4% at 60 lph. It could be
389 surmised that the energy losses associated with the volumetric absorption system reduces
390 with the flow rate while employing nanofluid, while the generated entropy during the gain of
391 heat from the sun increases with the flow rate. The increase in overall generation of entropy
392 is attributed to the development of temperature drop between the top wall of the collector and
393 the outlet due to the enhanced heat gain [27]. In addition, unlike the surface absorption based
394 parabolic collector, in volumetric absorption solar collector the working fluid directly absorbs
395 and convert the solar irradiance. Since the absorbing medium is in a kinematic state, the flow
396 rate directly affects the conversion of solar energy to heat. At higher flow rate of working
397 fluid, the energy conversion might be incomplete due to the insufficient time available for the
398 energy absorption owing to the rapid motion of nanoparticles in the working fluid.



399

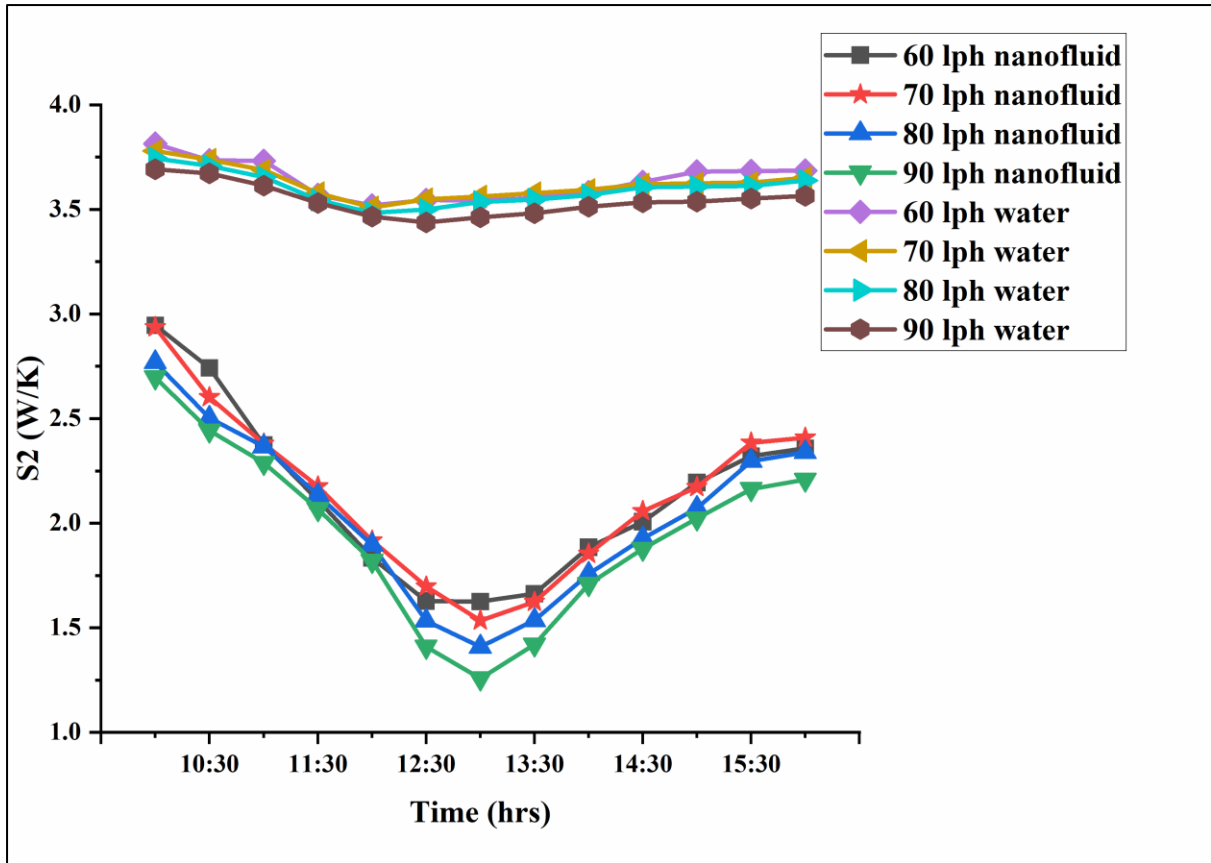
400

Fig. 9. Variation of average S1 and S2 with various flowrate.



401

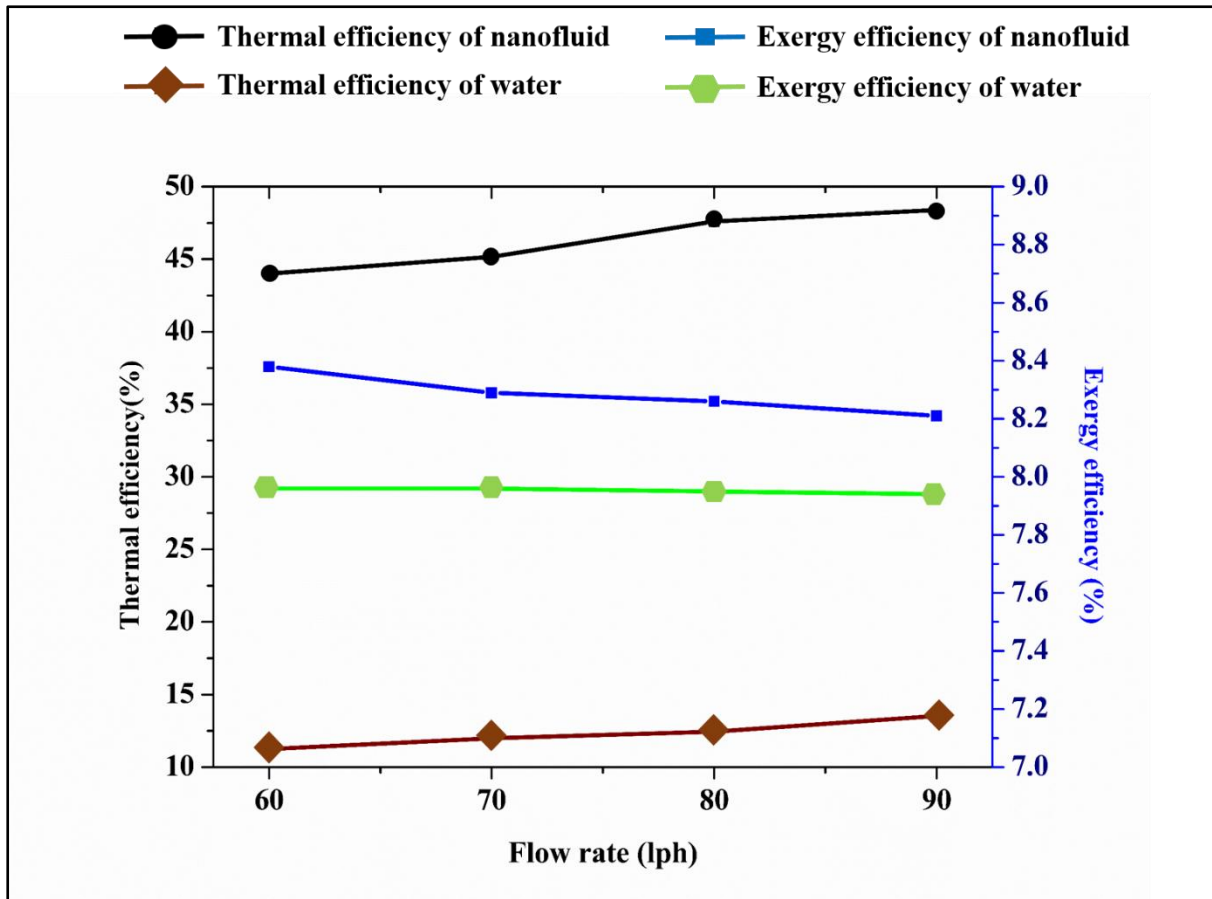
402 Fig.10: Instantaneous S1 of nanofluid and water at various flow rates.



403

404 **Fig. 11.** Instantaneous S2 of nanofluid and water at various flow rates.

405



406
407 **Fig. 12.** Thermal efficiency and exergy efficiency at various flowrate.

408 **Table 5. Maximum temperature difference, thermal efficiency and exergy efficiency**
409 **obtained for nanofluid and base fluid.**

Flow rate (lph)	Temperature Difference (K)		Thermal Efficiency (%)		Exergy efficiency (%)	
	Base fluid	Nanofluid	Base fluid	Nanofluid	Base Fluid	Nanofluid
60	2.71	10.8	13.80	55.01	7.97	8.64
70	2.46	10.01	14.55	59.23	7.96	8.59
80	2.21	9.06	14.96	61.34	7.95	8.52
90	2.08	8.41	15.86	64.12	7.95	8.48

410

411 **4. Conclusion**

412 The study demonstrates the favourable influence of binary SiO₂/Ag-CuO nanofluid on
413 augmenting the performance of volumetric absorption parabolic solar collector. The
414 constituents in the nanofluid was optimised using the response surface methodology and
415 desirability function. Nanofluid of optimum constituents (RTC of 1.234 and SRAF of

416 82.84%) was used as the working fluid in the volumetric absorption parabolic solar collector
417 and the effect of flow rate on various performance parameters were estimated. The major
418 findings are summarised as follows:

- 419 • A maximum temperature difference of 10.8K was observed for nanofluid at 60lph and
420 8.41K at 90 lph.
- 421 • SiO₂/Ag-CuO nanofluid improved the thermal performance of the collector with a
422 maximum overall enhancement of 48.74% in thermal efficiency noted at a flow rate
423 of 90lph.
- 424 • Increase in the flow rate leads to enhanced thermal efficiency of the collector, the
425 maximum thermal efficiency of 55.01% and 64.12% were obtained at 60lph and
426 90lph.
- 427 • The presence of SiO₂/Ag-CuO nanofluid reduced the entropy generation and thus
428 improved the exergy efficiency of the collector. However, entropy generation
429 increased with the flow rate which in turn reduced the exergy efficiency.
- 430 • Exergy efficiency of collector using nanofluid was enhanced by 8.4% at 60 lph, in
431 comparison with water.

432 REFERENCES

- [1] Sanaz Akbarzadeh, Mohammad Sadegh Valipour, Heat transfer enhancement in parabolic trough collectors: A comprehensive review, *Renew Sustain Energy Rev* 92 (2018) 198–218
<https://doi.org/10.1016/j.rser.2018.04.093>
- [2] R. Jain, R. Pitchumani, Fabrication and characterization of multiscale, fractal textured solar selective coatings, *Sol. Energy Mater. Sol Cells* 172 (2017) 213–219
<https://doi.org/10.1016/j.solmat.2017.07.009>
- [3] G.C. Bakos, Ch. Tsechelidou Solar aided power generation of a 300 MW lignite fired power plant combined with line-focus parabolic trough collectors field, *Renewable Energy* 60 (2013) 540-547
<https://doi.org/10.1016/j.renene.2013.05.024>
- [4] Jian-ping Meng, Xiao-peng Liu, Zhi-qiang Fu, Ke Zhang, Optical design of Cu/Zr_{0.2}AlN_{0.8}/ZrN/AlN/ZrN/AlN/Al₃₄O₆₂N₄ solar selective absorbing coatings *Sol. Energy* 146 (2017) 430–435
<https://doi.org/10.1016/j.solener.2017.03.012>
- [5] Xiaoxiao Yu, Yimin Xuan, Investigation on thermo-optical properties of CuO/Ag plasmonic nanofluids, *Solar Energy* 160 (2018) 200–207.
<https://doi.org/10.1016/j.solener.2017.12.007>
- [6] Tahereh B. Gorji, A.A. Ranjbar, A review on optical properties and application of nanofluids in direct absorption solar collectors (DASCs), *Renew Sustain Energy Rev* 72 (2017) 10–32
<https://doi.org/10.1016/j.rser.2017.01.015>

- [7] Harriet Kimptona, Domenico Andrea Cristaldia, Eugen Stulzb, Xunli Zhang, Thermal performance and physicochemical stability of silver nanoprism based nanofluids for direct solar absorption, *Sol. Energy* 199 (2020) 366–376
<https://doi.org/10.1016/j.solener.2020.02.039>
- [8] Shiva Gorjian, Hossein Ebadi , Francesco Calise , Ashish Shukla , Carlo Ingraio, A review on recent advancements in performance enhancement techniques for low-temperature solar collectors, *Energy Convers. Manage* 222 (2020) 113246
<https://doi.org/10.1016/j.enconman.2020.113246>
- [9] Caiyan Qin, Joong Bae Kim, Bong Jae Lee, Performance analysis of a direct-absorption parabolic-trough solar collector using plasmonic nanofluids, *Renewable Energy* 143 (2019) 24-33
<https://doi.org/10.1016/j.renene.2019.04.146>
- [10] Vishal Bhalla, Sachin Beejawat, Jay Doshi, Vikrant Khullar, Harjit Singh, Himanshu Tyagi, Silicone oil envelope for enhancing the performance of nanofluid based direct absorption solar collectors, *Renewable Energy* 145 (2020) 2733-2740
<https://doi.org/10.1016/j.renene.2019.08.024>
- [11] Kongxiang Wang, Yan He, Pengyu Liu, Ankang Kan, Zhiheng Zheng, Lingling Wang, Huaqing Xie, Wei Yu, Highly-efficient nanofluid-based direct absorption solar collector enhanced by reverse-irradiation for medium temperature applications, *Renewable Energy* 159 (2020) 652-662
<https://doi.org/10.1016/j.renene.2020.05.167>
- [12] Ahmet Z.Sahin, Mohammed Ayaz Uddin, Bekir S.Yilbas, AbdullahAl-Sharafi Performance enhancement of solar energy systems using nanofluids: An updated review, *Renewable Energy* 145 (2020) 1126-1148
<https://doi.org/10.1016/j.renene.2019.06.108>
- [13] Sarkar J, Ghosh P, Adil A, A review on hybrid nanofluids: recent research, development and applications, *Renew Sustain Energy Rev* 43 (2015) 164–177
<https://doi.org/10.1016/j.rser.2014.11.023>
- [14] Vishal Bhalla, Vikrant Khullar, Himanshu Tyagi, Experimental investigation of photo-thermal analysis of blended nanoparticles ($\text{Al}_2\text{O}_3/\text{Co}_3\text{O}_4$) for direct absorption solar thermal collector, *Renewable Energy* 123 (2018) 616-626
<https://doi.org/10.1016/j.renene.2018.01.042>
- [15] Nan Chen, Haiyan Ma, Yang Li, Jinhu Cheng, Canying Zhang, Daxiong Wu, Haitao Zhu. Complementary optical absorption and enhanced solar thermal conversion of CuO-ATO nanofluids, *Sol. Energy Mater. Sol Cells*. 162 (2017) 83-92
<https://doi.org/10.1016/j.solmat.2016.12.049>
- [16] Jia Zeng, Yimin Xuan, Enhanced solar thermal conversion and thermal conduction of MWCNT-SiO₂/Ag binary nanofluids, *Appl. Energy*, 212 (15) (2018), 809-819
<https://doi.org/10.1016/j.apenergy.2017.12.083>
- [17] Pawel Keblinski, Jeffrey A. Eastman, David G. Cahill, Nanofluid for thermal transport, *Mater. Today*, 8 (6) (2005) 36-44
[https://doi.org/10.1016/S1369-7021\(05\)70936-6](https://doi.org/10.1016/S1369-7021(05)70936-6)
- [18] Nor Azwadi Che Sidik, Muhammad Mahmud Jamil, Wan Mohd Arif Aziz Japar, Isa Muhammad Adamu, A review on preparation methods, stability and applications of hybrid nanofluids, *Renew Sustain Energy Rev* 80 (2017) 1112-1122
<https://doi.org/10.1016/j.rser.2017.05.221>
- [19] Mikko Makela, Experimental design and response surface methodology in energy applications: A tutorial review, *Energy Convers. Manage*, 151 (2017) 630-640.
<https://doi.org/10.1016/j.enconman.2017.09.021>

- [20] Wenlian Ye, Peng Yang, Yingwen Liu, Multi-objective thermodynamic optimization of a free piston Stirling engine using response surface methodology, *Energy Convers. Manage* 176 (2018) 147–163
<https://doi.org/10.1016/j.enconman.2018.09.011>
- [21] Sreehari Sreekumar, Albin Joseph, C.S. Sujith Kumar, Shijo Thomas, Investigation on influence of antimony tin oxide/silver nanofluid on direct absorption parabolic solar collector, *J. Clean. Prod.* 249 (2019) 119378
<https://doi.org/10.1016/j.jclepro.2019.119378>
- [22] A. Kasaeian, S. Daviran, R. D. Azarian, A. Rashidi, 2015, Performance evaluation and nanofluid using capability study of a solar parabolic trough collector, *J. Clean. Prod.* 89 (2015) 368–375.
<https://doi.org/10.1016/j.enconman.2014.09.056>.
- [23] E. Bellos, C. Tzivanidis, Thermal analysis of parabolic trough collector operating with mono and hybrid nanofluids, *Sustain. Energy Technol. Assess.* 26 (2018) 105–115.
<https://doi.org/10.1016/j.seta.2017.10.005>
- [24] T.P. Otanicar, P.E. Phelan, J. S. Golden, Optical properties of liquids for direct absorption solar thermal energy systems, *Sol. Energy* 83 (2009) 969–977.
<https://doi.org/10.1016/j.solener.2008.12.009>.
- [25] Yong Yang Gan, Hwai Chyuan Ong, Tau Chuan Ling, N.W.M. Zulkifli, Chin-Tsan Wang, Yung-Chin Yang, Thermal conductivity optimization and entropy generation analysis of titanium dioxide nanofluid in evacuated tube solar collector, *Appl. Therm. Eng.* 145 (2018) 155–164.
<https://doi.org/10.1016/j.applthermaleng.2018.09.012>
- [26] Moffat, R.J., 1985. Describing the uncertainties in the experimental results. *Exp. Therm. Fluid Sci.* 1, 3–17.
[https://doi.org/10.1016/0894-1777\(88\)90043-X](https://doi.org/10.1016/0894-1777(88)90043-X).
- [27] Salma Parvin, Rehana Nasrin, M.A. Alim, Heat transfer and entropy generation through nanofluid filled direct absorption solar collector, *Int. J. Heat Mass Transfer* 71 (2014) 386–395.
<http://dx.doi.org/10.1016/j.ijheatmasstransfer.2013.12.043>
- [28] Albin Joseph, Sreehari Sreekumar, C S Sujith kumar, Shijo Thomas, Optimisation of thermo-optical properties of SiO₂/Ag-CuO nanofluid for direct absorption solar collectors, *J. Mol. Liq.* (2019) 111986.
<https://doi.org/10.1016/j.molliq.2019.111986>
- [29] T. Aguilar, E. Sani, L. Mercatelli, I. Carrillo-Berdugo, E. Torres, J. Navas, Exfoliated graphene oxide-based nanofluids with enhanced thermal and optical properties for solar collectors in concentrating solar power, *J. Mol. Liq* 306 (2020) 112682.
<https://doi.org/10.1016/j.molliq.2020.112862>
- [30] Omid Mahian, Ali Kianifar, Soteris A. Kalogirou, Ioan Pop, Somchai Wongwises, A review of the applications of nanofluids in solar energy, *Int. J. Heat Mass Transfer* 57 (2013) 582–594
<http://dx.doi.org/10.1016/j.ijheatmasstransfer.2012.10.037>
- [31] M.M. Heyhat, M. Valizade, Sh. Abdolahzade, M. Maerefat, Thermal efficiency enhancement of direct absorption parabolic trough solar collector (DAPTSC) by using nanofluid and metal foam, *Energy* 192 (2020) 116662
<https://doi.org/10.1016/j.energy.2019.116662>
- [32] M.A. Sharafeldin, Gyula Grof, Evacuated tube solar collector performance using

CeO₂/water, nanofluid, J. Clean. Prod 185 (2018) 347-356
<https://doi.org/10.1016/j.jclepro.2018.03.054>

433

1 **Energy and Exergy analysis of SiO₂/Ag-CuO plasmonic nanofluid on direct absorption**
2 **parabolic solar collector**

3 Albin Joseph^a, Sreehari Sreekumar^b, Shijo Thomas^{a*}

4 ^a School of Materials Science and Engineering, National Institute of Technology, Calicut
5 673601, India

6 ^b Department of Mechanical Engineering, National Institute of Technology, Calicut 673601,
7 India

8 Corresponding Author: Shijo Thomas, Email Address: shijo@nitc.ac.in

9 **ABSTRACT**

10 Experimental investigations on the application of SiO₂/Ag-CuO plasmonic nanofluid
11 on direct/volumetric absorption parabolic solar collectors is presented in this article. The
12 process variables for the preparation of nanofluid were optimised by employing the
13 desirability function and response surface methodology (RSM). The optimisation was
14 performed to achieve nanofluid with maximum possible thermal conductivity and solar
15 absorptivity. The final solar radiation absorbed fraction and relative thermal conductivity
16 noted for the optimised nanofluid was 82.84% and 1.234, respectively. The performance of
17 the collector was evaluated at various flow rates from 60 lph to 90 lph, using water and
18 optimised nanofluid as the heat transfer fluid. It is noted from the results that the thermal
19 efficiency of the collector increases with the flow rate whereas, the exergy efficiency
20 decreases for both water and nanofluid. The highest temperature difference of 11.27K was
21 noted at 60lph for nanofluid which corresponds to a thermal efficiency of 57.47%. A
22 maximum thermal efficiency of 64.05% was noted at 90 lph which corresponds to an
23 enhancement of 48.19 % in comparison with water. Exergy efficiency of the nanofluid was
24 enhanced by 9.4% at 60 lph, in comparison with water.

25

26 **Keywords:** Volumetric absorption parabolic solar collector, Binary nanofluid, Response
27 surface methodology, Thermal efficiency, Entropy generation.

28

29

30 **Nomenclature**

A	Area of parabola (m^2)	T_{in}	Inlet temperature (K)
A_p	Aperture width of parabola(m)	T_{sun}	Temperature of Sun (K)
C_p	Specific heat of working fluid (kJ/kg.K)	θ	Rim angle of the parabola
E_{des}	Energy destruction (W)	σ	Uncertainty
f	Focal length of the parabola (m)	τ_t	Transmittance of absorber tube
I	Solar irradiance (W/m^2)	r_r	Reflectivity of reflector
m	mass flow rate (kg/sec)	η_{ex}	Exergy efficiency
Q_u	Heat gained (W)	η_{th}	Thermal efficiency
Q_s	Available direct solar energy (W)	η_{opt}	Optical efficiency of the parabola
Q_o	Energy loss (W)	RSM	Response surface methodology
S_{gen}	Entropy generation (W/K)	RTC	Relative thermal conductivity
T_{amb}	Ambient temperature (K)	SRAF	Solar radiation absorbed fraction
		S1	Entropy generated during the transfer of heat to working fluid from solar irradiance
T_{out}	Outlet temperature (K)	S2	Entropy generated during the heat loss

31

32 **1. Introduction**

33 The persistent consumption of fossil fuels made them insufficient to meet the
 34 overwhelmingly increasing demand of energy. Stepping up the utilisation of sustainable
 35 energy sources is a widely acknowledged optimistic solution to meet the ever augmenting
 36 need for energy. Solar energy, a potential replacement to fossil fuels, provides high hope to
 37 overcome the energy crisis to a certain extent, especially in electricity generation and various
 38 heating application [1]. Solar energy being a sustainable and clean source of energy is
 39 gaining widespread attention for many thermal applications. A number of studies have been
 40 reported based on the solar energy conversions like solar thermal conversion, photo electric
 41 conversion and photo electric thermal conversion. The solar thermal convertors like dish
 42 collector, linear Fresnel reflectors (LFR) and parabolic trough collector (PTC) are the most
 43 preferred techniques for the medium and high temperature applications. In these techniques
 44 solar radiation is concentrated to a line or a point from which it is transferred to the working
 45 fluid (heat transfer fluid). Parabolic collectors are widely used for solar thermal application
 46 due to its better performance and comparative cost effectiveness. A parabolic trough
 47 collector is equipped with three components mainly, the parabolic reflector plate equipped
 48 with an absorber tube at its focal point and the working fluid inside the absorber tube. In a

49 typical operation of parabolic collector, solar ray is concentrated (using a parabolic reflector)
50 towards the receiver tube placed at the focal line of the reflector, from which the converted
51 energy in the form of heat is transferred by a working fluid for various applications like water
52 heating, space heating, solar refrigeration system and even for power generation [2]. The
53 solar thermal collectors could be coupled with various thermal systems like power generators,
54 in order to improve the efficiency of the whole unit. Bakos and Tsehelidou [3] investigated
55 solar trough collector coupled with the lignite fired steam power plant using a TRNSYS
56 simulation software. They found that the Rankine efficiency of the plant improved from 33%
57 to 37.64%. They also claim that the solar power plant could reduce the total fuel consumption
58 and thus the CO₂ emission.

59 Apart from the design parameters of the parabolic collector, researchers now a
60 days are focusing on the modification of absorber tubes. Solar absorptivity of the absorber
61 tube is an important parameter that influences the performance of the collector [4, 23]. The
62 absorber tube is an intermediate between the solar radiation and the working fluid. The
63 absorption of solar energy will heat up the absorber tube. This heat is then conducted from
64 the outer surface to the inner surface of the absorber tube which then is transferred to the heat
65 transfer fluid/working fluid through convection. The intermediate heat losses through
66 convection and radiation from the hot absorber tube surface to ambient, results in a
67 deterioration in the performance of the collector [5, 22, 24]. This is where the concept of
68 direct/volumetric absorption solar collectors gains significance by significantly reducing the
69 thermal losses since the photo thermal conversion is directly achieved by the heat transfer
70 fluid/working fluid [6]. Solar radiation absorption capability of the working fluid is the metric
71 of performance of the volumetric absorption solar thermal conversion systems. The poor
72 solar absorptivity of commonly used working fluids like deionised water, ethylene glycol,
73 thermal oils, etc. renders them unfit for direct application in direct absorption collectors.
74 Improving the solar absorptivity of these fluids is an area of active research [7, 8].

75 Nanofluids, with enhanced optical properties, are a suitable replacement for
76 conventional heat transfer fluid in volumetric absorption solar collectors. Qin, et al. [9] made a
77 performance evaluation of novel volumetric solar absorption parabolic collector using
78 plasmonic nanofluids with constant absorption coefficient. An additional reflective coating
79 was given on the upper half of the receiver tube that enhances the optical path length and
80 investigations were performed by varying the receiver tube diameter. They concluded that
81 thermal efficiency of the collector reduced with the diameter and at optimal diameter the
82 direct absorption collector exhibit better performance than the conventional collectors. The

83 authors also claim that direct absorption parabolic collectors are effective at low flowrate
84 (≤ 0.18 kg/s). As per the reports of Bhalla et al. [10] a layer of silicon envelope over the
85 nanofluids could reduce the thermal losses due to convection to the atmosphere. The
86 enhancement on temperature was nearly 3.5°C . Wang et al. [11] introduced a novel technique
87 which improved the efficiency of the direct absorption collector by introducing reverse
88 irradiation. As per their observation the temperature within the fluid was almost uniform
89 compared to the directed irradiated system, which establishes the influence of the
90 nanoparticles in the fluid. However, the enhancement in the properties of nanofluid is limited
91 up to a critical concentration, beyond which the properties of the nanofluid drops. The reason
92 is attributed to reduced stability of the nanofluid at higher concentrations due to the
93 agglomeration and sedimentation of the nanoparticles [28]. Recent reports [12] reveals that
94 binary nanofluids exhibits better properties as compared to conventional nanofluids, due to
95 the combined effect of two or more particles [13]. Bhalla at al. [14] investigated the influence
96 of $\text{Al}_2\text{O}_3/\text{Co}_3\text{O}_4$ binary nanofluid on direct solar absorption system and compared it with that
97 of the surface absorption system. The authors noticed 5.4°C rise in the temperature for
98 optimum direct absorption fluid compared to the surface absorption system. The reports of
99 Chen et al. [15] reveals that improved optical properties are noted for binary nanofluid in
100 which a broad absorption of solar radiation was observed. Zeng and Xuan [16] reports that
101 the plasmonic effect of noble nanoparticles exhibits high photo thermal conversion. SiO_2/Ag
102 is one of the commonly used plasmonic nanoparticles. However, the hybrid nanoparticles are
103 found to be larger in size due to which the stability of the nanofluid is affected highly. As per
104 the reports of Keblinski et al. [17] the particles size have very high impact on stability and
105 properties of the nanofluid. The improved effectiveness of the nanofluid is observed at lower
106 particle size. Thermo-optical properties of the nanofluid have very high significance in the
107 direct absorption solar collector [29, 30]. Due to this reason it is highly recommended to
108 employ working fluid with high thermal and optical properties in volumetric absorption solar
109 collectors. From these perspectives, it is clear that the binary nanofluid in which more than
110 one nanoparticles are dispersed, is capable to achieve both. The colloidal stability of the
111 nanoparticles in the fluid is one of the main practical drawback associated with nanofluids.
112 Nevertheless, this issue can be addressed by various methods like addition of surfactants,
113 varying pH of the fluid, surface functionalization of the nanoparticles, etc. By enhancing the
114 mutual repulsion between the particles, the chance of agglomeration of the particles and
115 further sedimentation can be prevented. Zeta potential analysis is one of the method used to
116 quantify the colloidal stability of nanofluids. An absolute value of zeta potential greater the

117 30 mv is considered to yield a stable nanofluid. However, for flow applications the issue of
118 the stability is less pronounced since the fluid under circulation is in continuous agitation
119 [18].

120 In the present study the performance evaluation of the volumetric absorption collector
121 using plasmonic SiO₂/Ag-CuO binary nanofluid is investigated experimentally. Additional
122 advantages on photo-thermal conversion of nanofluid could be observed in SiO₂/Ag particles
123 due to the plasmonic effect, the thermal transport within the nanofluid is being influenced by
124 the CuO nanoparticles. The desirability function combined with the response surface
125 methodology (RSM), a widely adopted technique in industries for multi objective response
126 process, was used to optimise the process variables involved in the study [19, 20]. The
127 experiments were conducted at National Institute of Technology Calicut (latitude: 11.3216,
128 longitude: 75.9336). Thermo-optical properties exhibited by the nanofluid as well as the
129 collector efficiency and entropy generation of the collector are analysed using the optimised
130 SiO₂/Ag-CuO nanofluid, and compared with base fluid. Even though many lab scale studies
131 on the optical properties of plasmonic nanofluid were reported, to the best of the author's
132 knowledge this is the first attempt that investigates the influence of a plasmonic binary
133 nanofluid on a volumetric absorption parabolic collector.

134 **2. Materials and methods**

135 *2.1 Synthesis of SiO₂/Ag-CuO nanofluid.*

136 SiO₂/Ag-CuO nanofluid was synthesised by two step method in which the particles
137 are added and dispersed in the water. SiO₂/Ag particle used in the fluid was prepared by
138 introducing Ag on the SiO₂ by reducing AgNO₃ with SnCl₂. CuO nanoparticles used are
139 directly purchased from Sigma Aldrich. To achieve a stable suspension, sodium dodecyl
140 sulfonate was used as surfactant. Optimisation of the concentration of nanoparticle and
141 surfactant were done using a desirability function. The detailed procedure of synthesis of
142 nanofluid and optimisation is mentioned in the earlier investigation conducted by the same
143 authors [28]. The optimised nanofluid is then used in the volumetric absorption solar
144 collector.

145 *2.2. Design and manufacturing of experimental setup.*

146 *2.2.1 Parabolic reflector*

147 The length of parabolic trough is 1500 mm and the aperture width is 1080 mm. Three
 148 troughs of dimensions 500 mm length and 1080mm aperture diameter each were fabricated
 149 using the glass wool - epoxy composite. Anodised aluminium sheets were used as the
 150 reflector. The reflector sheets were fixed on the glass wool-epoxy composite parabolic trough
 151 so that the reflector attain the parabolic trough shape. The rim angle of the parabola is 90° and
 152 Eq. 1 represents the parabolic profile of the fabricated trough.

$$153 \quad Y = 0.925X^2 \quad (1)$$

154 The focal point of the parabola is given by equation 2

$$155 \quad f = \frac{Ap}{2} \cot\theta + \frac{Ap^2}{16f} \quad (2)$$

156 Where f is focal length of the parabola, θ is the rim angle and A_p , the aperture width of the
 157 parabola.

158 The dimensions of the parabolic trough are presented in Table 1.

159 **Table. 1: Dimension of parabolic trough fabricated.**

Parameter	Dimension
Length of parabola	1.5 m
Distance of focal point	0.272 m
Aperture width	1.05m
Aperture Area	1.575 m ²
Rim angle	90°
Outer tube inner diameter	0.035 m
Inner tube inner diameter	0.015 m

160

161 2.2.2 Absorber Tube.

162 Optical absorptivity and other dimensions of the absorber tube highly influences the
 163 thermal and optical efficiency of a parabolic solar collector. In the present system, glass-glass
 164 absorber tube made of quartz is used, which enable high transmittance, reducing the optical
 165 losses of absorber tube. Moreover, the evacuation of glass- glass annulus could reduce the
 166 convective heat losses [10]. A provision was made on the experimental setup to adjust the
 167 position of the absorber tube so as to maintain the absorber tube exactly at the focal point of

168 the parabolic trough. Both ends of the absorber tube were sealed using Teflon coupling which
169 could withstand temperature up to 350°C and high temperature RTV silicon (anabond) was
170 used as sealant.

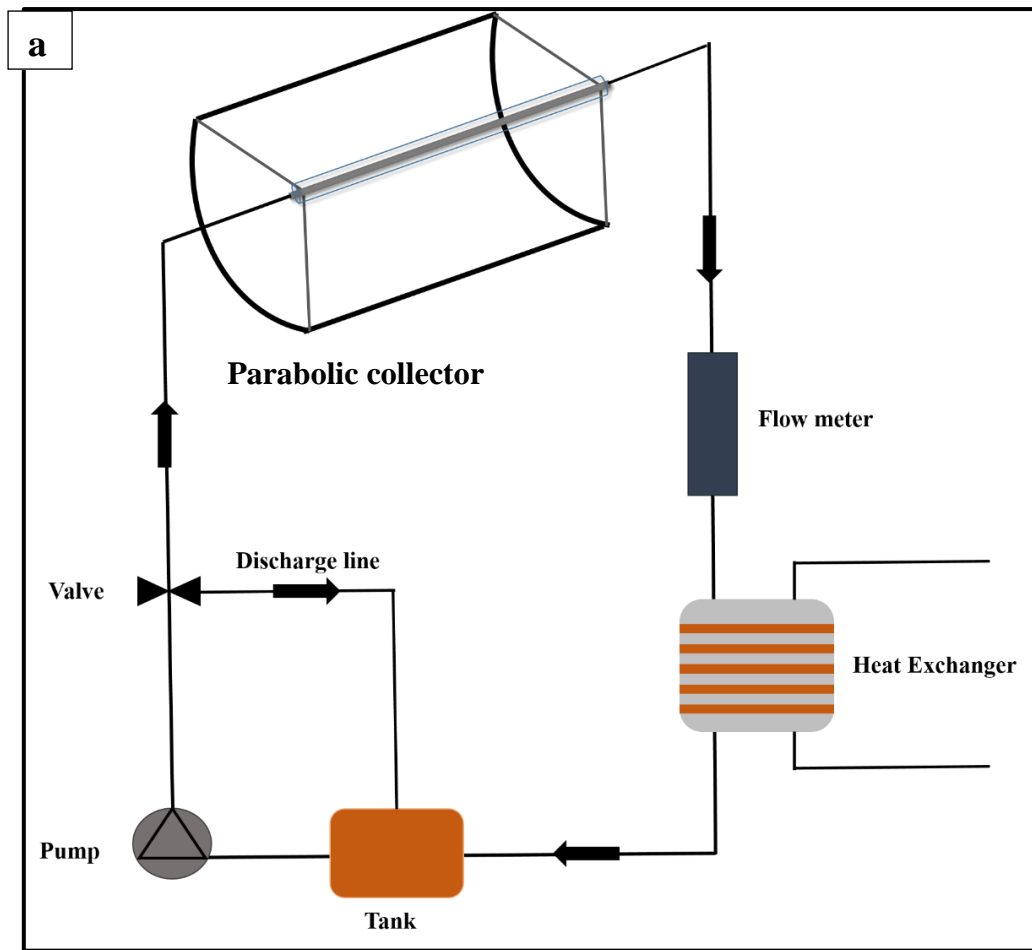
171 *2.2.3 Solar Tracker*

172 Continuous tracking of sun is mandatory for the collector to get perpendicular rays on
173 its surface. To accomplish this a solar tracker was employed. The tracker consist of a geared
174 motor which is connected to the axis of parabolic collector. The sun tracking was achieved
175 using an LDR photo resister as the sensor. The LDR sensor unit (not clear in the figure due to
176 its small size) placed on the trough is connected to geared motor unit with an intermediate
177 PCB circuit.

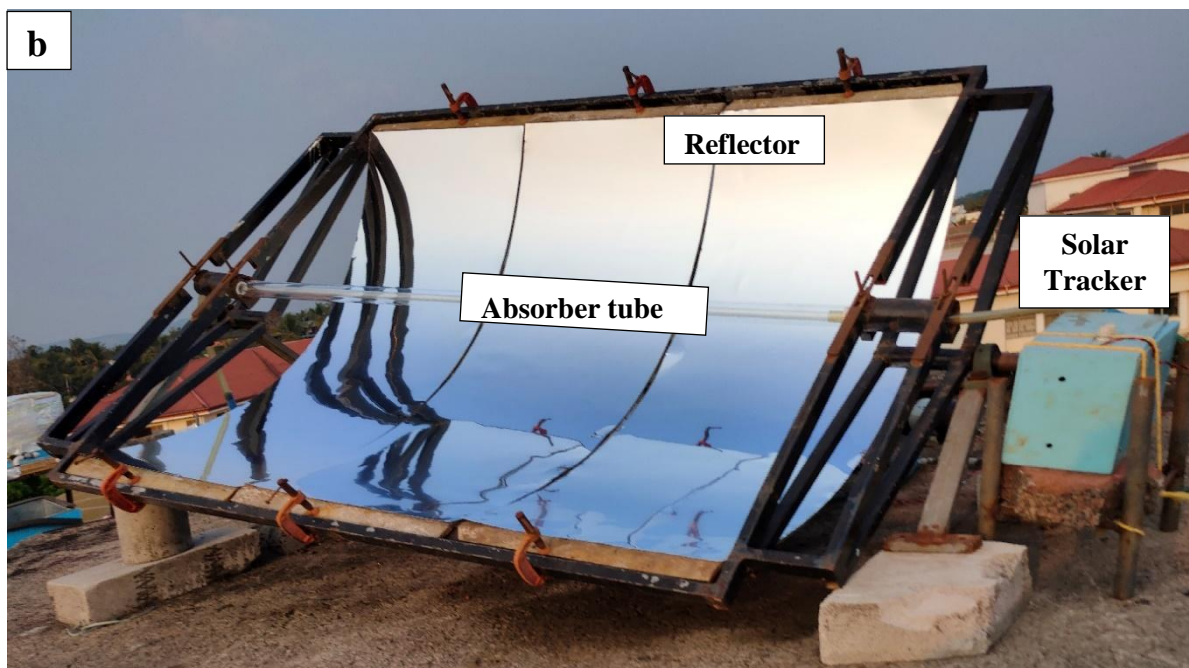
178 *2.2.4 Experimental procedure.*

179 The parabolic trough collector used in the present study is located at National Institute
180 of Technology, Calicut in the North-South direction (latitude: 11.3216, longitude: 75.9336).
181 The experiment was carried out on clear sunny days during the month of March and April.
182 The hydraulic cycle chosen for the study is shown in Fig 1. According to Fig 1 the nanofluid
183 from a reservoir is pumped to the parabolic collector and then to a heat exchanging unit
184 (constant temperature bath). The heat exchanger cools the nanofluid and maintain a constant
185 temperature at the inlet of absorber tube. The nanofluid from the heat exchanger is finally
186 directed to the reservoir. The flow rate of the nanofluid was varied using a valve and flow
187 meter. The inlet and outlet temperatures were noted using calibrated T-type thermocouples,
188 connected to a data logger (Agilent). The temperatures were noted at every 5 minutes interval
189 from 09:45 am to 4:15 pm and average temperature for every 30 minutes were determined.

190 As mentioned in Section 2.2 the nanofluid was synthesised based on the range of
191 concentration mentioned in Table 3 and its thermo-optical properties were measured. An
192 optimised process variables of nanofluids were achieved that enables maximum possible
193 solar radiation absorption and thermal conductivity. The nanofluid prepared using this
194 optimised combination is further experimentally analysed to quantify its effect on volumetric
195 absorption parabolic collector (VAPC). The influence of this nanofluid on VAPC at various
196 flow rates starting from 60 lph to 90 lph, were analysed and compared with that of base fluid.



197



198

199 Fig. 1. a) Schematic of experimental setup, b) Photograph of fabricated parabolic trough

200

201 *2.3 Mathematical formulation*

202 Mathematical formulation used for the estimation of performance parameters are listed
203 below:

204 Useful heat produced (W):

205
$$Q_u = m \cdot Cp \cdot (T_{out} - T_{in}) \quad (3)$$

206 Available direct solar energy:

207
$$Q_s = A \cdot I \quad (4)$$

208 Optical and thermal efficiency of the parabola was calculated using equation 5 and 6

209
$$\eta_{opt} = \tau_t r_r \quad (5)$$

210
$$\eta_{th} = \frac{Q_u}{Q_s} \quad (6)$$

211 Entropy generation (W/K):

212
$$S_{gen} = mCp \ln\left(\frac{T_{out}}{T_{in}}\right) - \frac{Q_s}{T_{sun}} + \frac{Q_o}{T_{amb}} \quad (7)$$

213 The entropy generation during the heat transfer from sun to nanofluid and inside absorber
214 tube was estimated using Eq 7. The entropy generated due to the pressure drop during fluid
215 flow is neglected as it was insignificant.

216
$$Q_o = Q_s - mCp (T_{out} - T_{in}) \quad (8)$$

217 Energy destruction (W):

218
$$E_{des} = S_{gen} \times T_{amb} \quad (9)$$

219 Exergy efficiency:

220
$$\eta_{Ex} = 1 - \frac{T_{amb} \times S_{gen}}{\left[1 - \frac{T_{amb}}{T_{sun}}\right] Q_s} \quad (10)$$

221

222

223 *2.4 Experimental Uncertainty Analysis*

224 The uncertainty experimental data was estimated using the method described by Moffat [26].
 225 Table 2 presents the estimated uncertainty of various parameters. The calibration of
 226 thermocouple was done by employing a constant temperature bath as standard. The
 227 maximum error in the thermocouple was found to be $\pm 0.1\text{K}$, the uncertainty of Heat gained,
 228 thermal and exergy efficiency was calculated from the equation 11-13

$$229 \quad \frac{\sigma Qu}{Qu} = \sqrt{\left(\frac{\sigma m}{m}\right)^2 + \left(\frac{\sigma T_{in}}{T_{in}}\right)^2 + \left(\frac{\sigma T_{out}}{T_{out}}\right)^2} \quad 11$$

$$230 \quad \frac{\sigma \eta_{th}}{\eta_{th}} = \sqrt{\left(\frac{\sigma m}{m}\right)^2 + \left(\frac{\sigma T_{in}}{T_{in}}\right)^2 + \left(\frac{\sigma T_{out}}{T_{out}}\right)^2 + \left(\frac{\sigma I}{I}\right)^2} \quad 12$$

$$231 \quad \frac{\sigma \eta_{Ex}}{\eta_{Ex}} = \sqrt{\left(\frac{\sigma m}{m}\right)^2 + \left(\frac{\sigma T_{in}}{T_{in}}\right)^2 + \left(\frac{\sigma T_{out}}{T_{out}}\right)^2 + \left(\frac{\sigma T_{amb}}{T_{amb}}\right)^2 + \left(\frac{\sigma I}{I}\right)^2} \quad 13$$

232 **Table. 2: Uncertainties of variables**

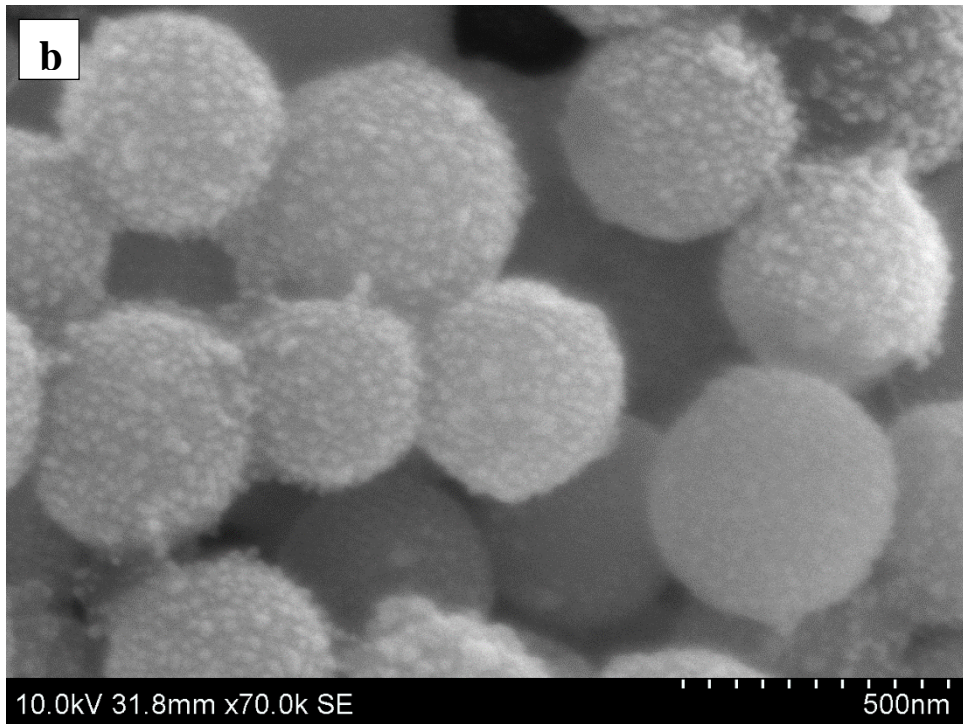
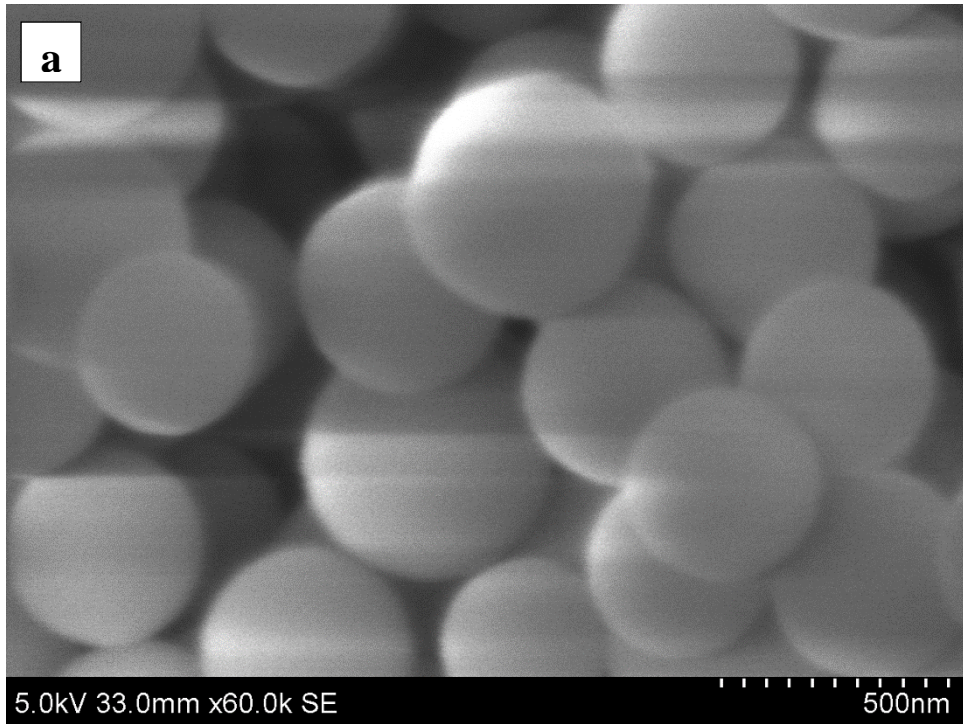
Variables	Uncertainty
Flow rate	$\leq \pm 2.5 \%$
Solar irradiance	$\leq \pm 5.00 \text{ W/m}^2$
Heat Gained	$\leq \pm 2.53 \%$
Thermal efficiency	$\leq \pm 2.6 \%$
Exergy efficiency	$\leq \pm 2.62 \%$

233

234 **3. Result and discussion**

235 *3.1 Characterisation of nanofluids*

236 Characterisation was limited to measurement of solar absorptivity and thermal
 237 conductivity of nanofluid and morphological analysis of nanoparticles. Data obtained from
 238 the UV-vis spectrometer (Avantes) was used to estimate the solar radiation absorbed fraction
 239 (SRAF). To quantify the thermal conductivity exhibited by the nanofluids, a thermal
 240 properties analyser (KD2 pro) was employed. Morphology of the nanoparticles were analysed
 241 using the field emission scanning electron microscope (Hitachi SU 6600) and are presented in
 242 Fig 2.



245 **Fig. 2.** SEM images a) SiO₂, b) SiO₂/Ag nanoparticles.

246 *3.2 Optimisation of SiO₂/Ag-CuO plasmonic binary nanofluid*

247 The optimisation of the nanofluid is detailed in the earlier publication by the same
248 authors [28]. Desirability approach on RSM was adopted to optimise the process variables
249 involved in the synthesis of nanofluid. Desirability function is a widely adopted approaches

250 to optimise multi objective problems [20]. The regression equation for relative thermal
 251 conductivity and SRAF obtained from the central composite design of response surface
 252 methodology (Eq. 14 and 15) was taken for the desirability approach [28]. The objective of
 253 the optimisation was to maximise SRAF and thermal conductivity of the nanofluids. In this
 254 approach the variables such as mass of nanoparticles like SiO₂/Ag and CuO, surfactant are in
 255 the design range (between upper limit and lower limit), while the responses like thermal
 256 conductivity and SRAF are set to be maximal. Table 3 presents the goal, lower and upper
 257 limit and importance of each process variables. The optimal combination of process variables
 258 was obtained as 206.3 mg of SiO₂/Ag per litre of DI water and correspondingly, 864.7 and
 259 1996.2 mg of CuO and SDS respectively. Figure 3 shows the variation of desirability with
 260 change in concentration of particles. It can be seen that, the desirability drops after
 261 concentration of SiO₂/Ag particles exceeds 206.3 mg/l, which might be due to the fact that
 262 beyond this concentration the stability of the nanofluid decreases resulting in a decrease in
 263 thermal conductivity and SRAF. However, the desirability increased with the concentration
 264 of CuO and then drops after 864.7mg/l. This could be due to the fact that, as the CuO
 265 concentration increases the thermo-optical properties are found to be increased and after a
 266 critical concentration the stability of the nanofluid was affected, thus decreasing the
 267 desirability. Moreover, the stability was found to be increased with surfactant concentration
 268 due to which the desirability increases with the concentration of surfactant. The optimised
 269 concentrations of nanoparticles were found to be stable with a zeta potential of -38.7mV. The
 270 RTC and SRAF for the optimised concentration were found to be 1.234 and 82.84%
 271 respectively from the response equations. To confirm this experimentally, the optimised
 272 nanofluid combination was prepared and the experimental value of RTC and SRAF were
 273 obtained as 1.231 and 81.79% respectively. Since the predicted and experimental values are
 274 comparable to each other in addition with the desirability value of one, the results are
 275 reliable. The final optimised nanofluid is then taken to the parabolic collector for the analysis
 276 of photo thermal conversion and entropy generation. In addition thermal conductivity of the
 277 optimised nanofluid in the temperature range, 30°C to 50°C, was measured and presented in
 278 the Table 4. The relative thermal conductivity (Thermal conductivity of nanofluid by thermal
 279 conductivity of water) was also estimated.

280 .

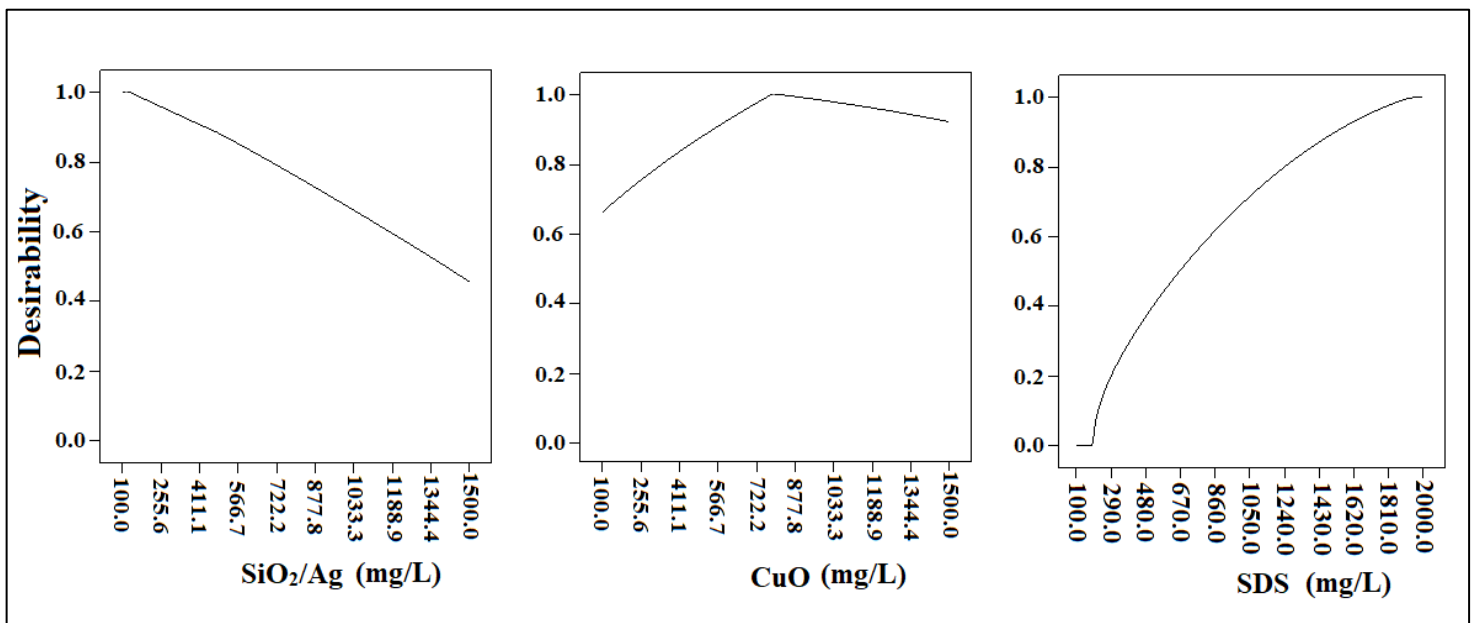
$$\begin{aligned}
 281 \text{ RTC} &= 1.11825 + (4.64016 \times 10^{-005} \times C) + (8.23773 \times 10^{-006} \times B) - (7.08371 \times 10^{-005} \times A) - \\
 282 &(2.81400 \times 10^{-008} \times A \times B) + (7.00727 \times 10^{-008} \times B \times C) - (1.48865 \times 10^{-008} \times A \times C) -
 \end{aligned}$$

283 $(1.87837 \times 10^{-008} \times C^2) - (6.43326 \times 10^{-009} \times B^2) + (3.11178 \times 10^{-008} \times A^2)$
 284 (14)

285 $SRAF = 35.2379 + (0.039759 \times C) + (0.010745 \times B) + (0.021866 \times A) - (3.34793E-006 \times A$
 286 $\times B) - (6.48624 \times 10^{-006} \times B \times C) - (6.67764 \times 10^{-006} \times A \times C) - (7.30303 \times 10^{-006} \times C^2) -$
 287 $(1.95099 \times 10^{-006} \times B^2) - (1.08898 \times 10^{-005} \times A^2)$
 288 (15)

289 Where A, B, and C are mass of SiO₂/Ag, CuO and SDS respectively per litre of DI water.

290



292 **Fig .3.** Variation of desirability function with process variables.

293 **Table. 3:** Conditions adopted during the optimisation.

Name	Goal	Lower limit	Upper limit	Importance
Concentration of SiO ₂ /Ag (mg/l)	In range	100	1500	4
Concentration of CuO (mg/l)	In range	100	1500	4
Concentration of SDS (mg/l)	In range	100	2000	4

294

295

296 **Table 4.** Thermal conductivity at various temperature

Temperature (°C)	Relative thermal conductivity	Thermal conductivity (W/mK)
30	1.234	0.7404
35	1.248	0.7491
40	1.262	0.7576
45	1.299	0.7794
50	1.314	0.7886

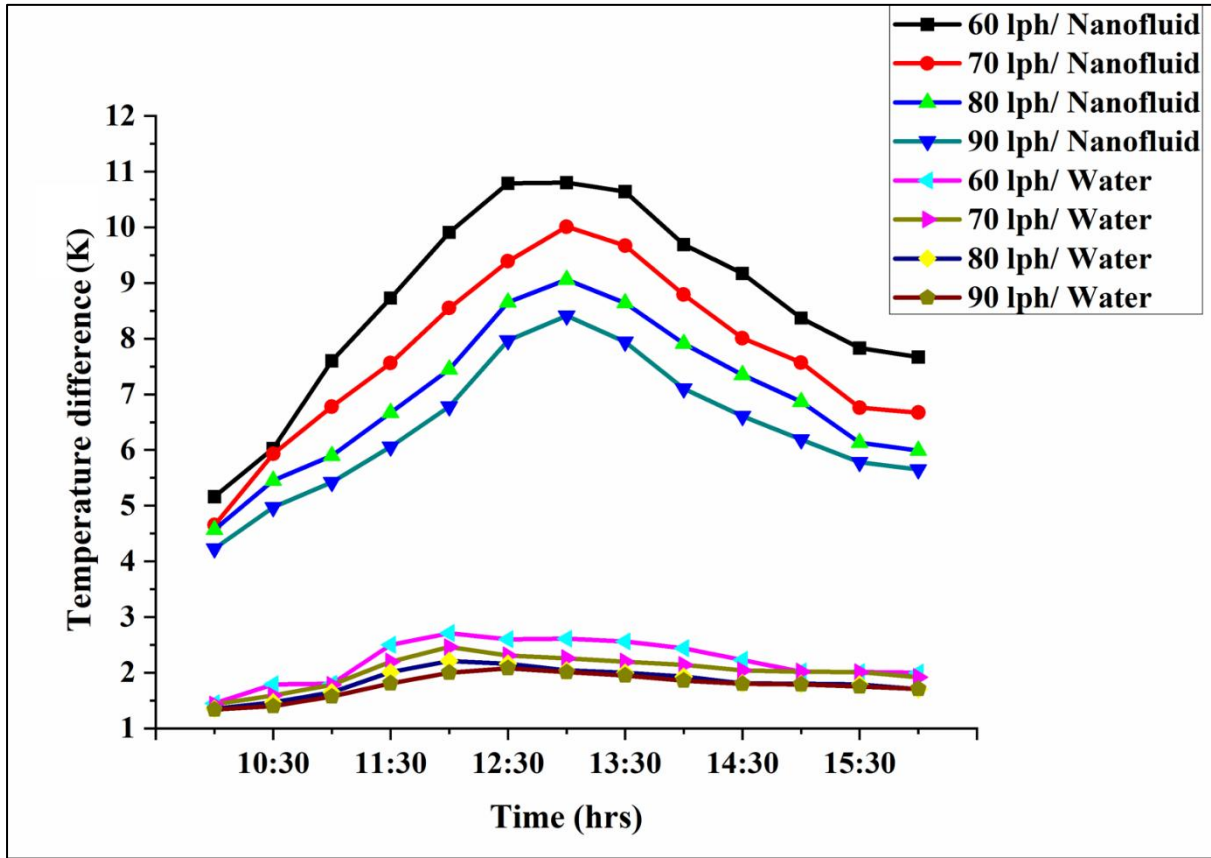
297

298 **3.3 Performance of SiO₂/Ag-CuO hybrid plasmonic nanofluid on parabolic collector.**

299 The SiO₂/Ag-CuO nanofluid used as working fluid in the parabolic collector was
 300 prepared based on the optimum process variables achieved from the procedure mentioned in
 301 3.2. The optimised valued of mass of particles and surfactant (process variables for preparing
 302 the nanofluid) are 206.3 mg/L, 864.7mg/L and 1996.2mg/L of SiO₂/Ag, CuO and SDS
 303 respectively. The experiment was carried out on a sunny day during the month of March and
 304 April. The Average solar radiation in the experimental location was 850 W/m². The
 305 maximum radiation noted was 950W/m² which mostly occur during 12:00 pm to 2:00 pm.

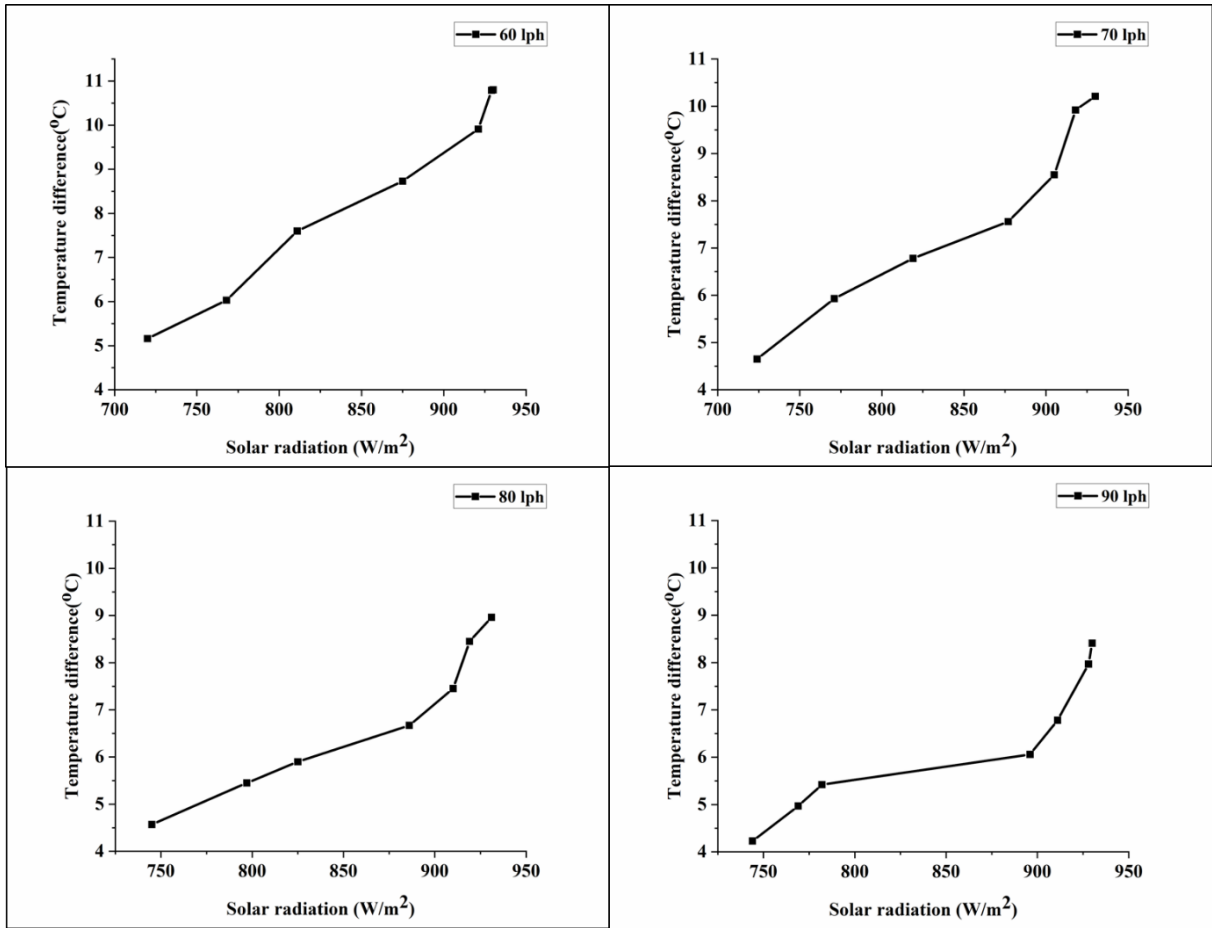
306 Figure 4 presents the temperature profile of nanofluid and the base fluid at various
 307 flow rates. The temperatures were noted from 10:00 am to 4:00 pm. As the figure says the
 308 temperature difference decreases with the increase in flow rate of working fluid. A maximum
 309 temperature difference of 11.27K was noted for the optimum nanofluid at the flow rate of 60
 310 lph and 8.4K at 90 lph. The highest noted temperature difference for water was 2.61K, at
 311 60lph. Table 4 shows the maximum temperature difference obtained for SiO₂/Ag-CuO
 312 nanofluid and water at various flow rates. It is apparent that the introduction of nanoparticles
 313 enhanced the performance of the collector by improving the optical and thermal properties of
 314 the nanofluid. The improved solar absorptivity of the nanofluid increased the solar thermal
 315 conversion of the collector and the enhancement in thermal conductivity augmented the heat
 316 transfer for nanofluids. The experiments were repeated three times and the reported values
 317 are the average, to ensure the repeatability. The variation of temperature difference with solar
 318 radiation is plotted and added in the manuscript as Figure 5. As can be seen form the figure
 319 the temperature difference increases with the solar radiation for a particular flow rate and the
 320 variation is almost linear. At a flow rate of 60 lph, the maximum temperature difference
 321 obtained was 10.8 °C for 930 W/m². The minimum temperature difference observed at this
 322 flow rate was 5.16 °C at a solar radiation of 720 W/m². The maximum temperature noted at
 323 90 lph was 8.41 °C at 930 W/m² for which the maximum efficiency was also obtained. The

324 maximum observed temperatures were 10.21 °C and 8.96 °C at flow rates of 70 and 80 lph
325 respectively for a solar radiation of 930 W/m²



326

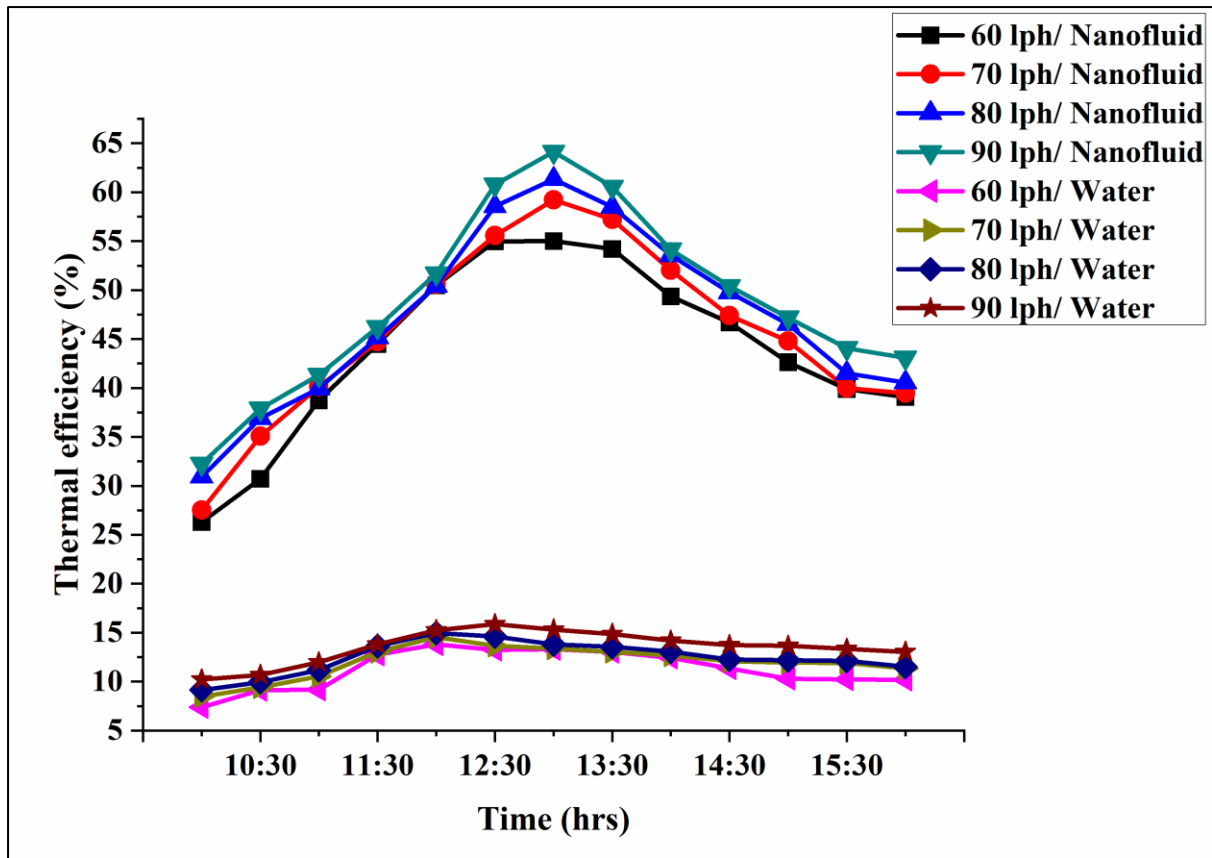
327 **Fig. 4.** Temperature profile of nanofluid and water at various flow rates.



328

329 **Fig. 5** Variation of temperature difference with radiation.

330



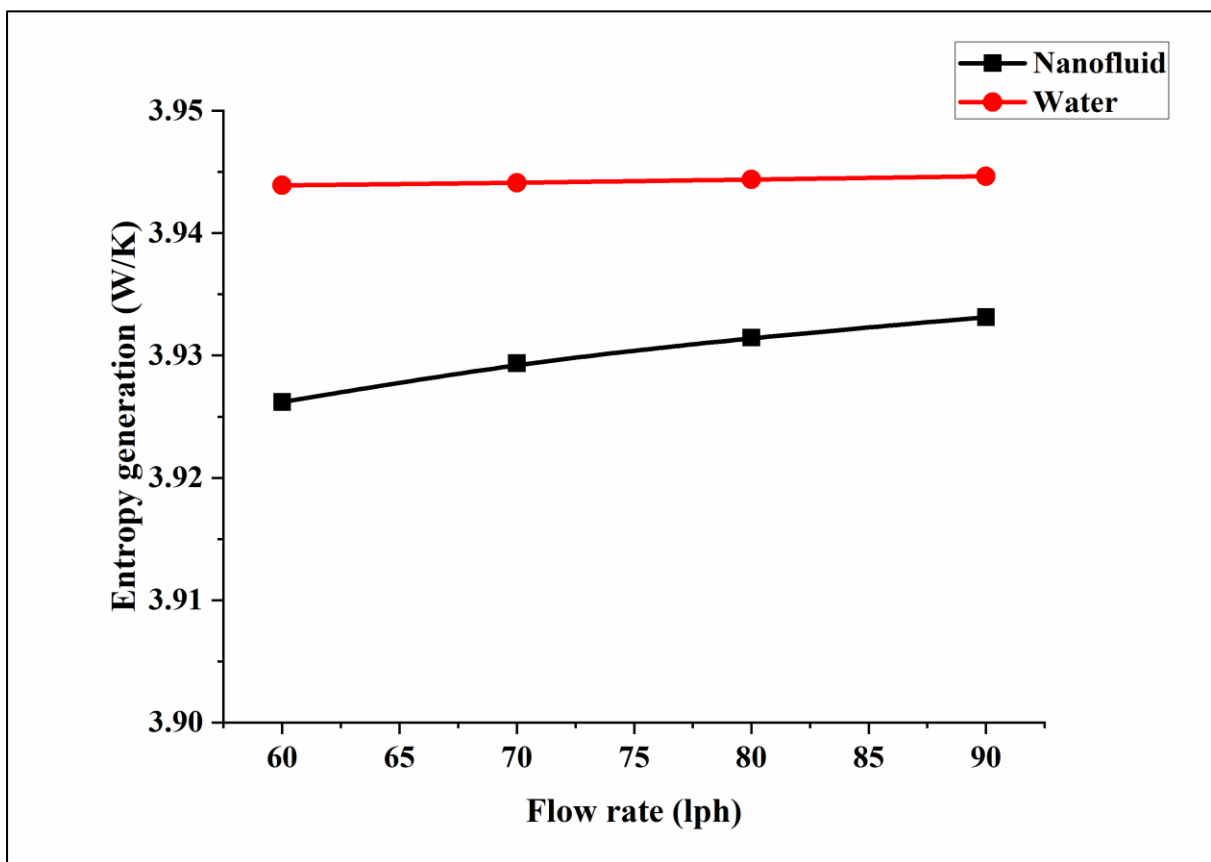
331

332 **Fig. 6.** Thermal efficiency plot of nanofluid and water at various flow rates.

333

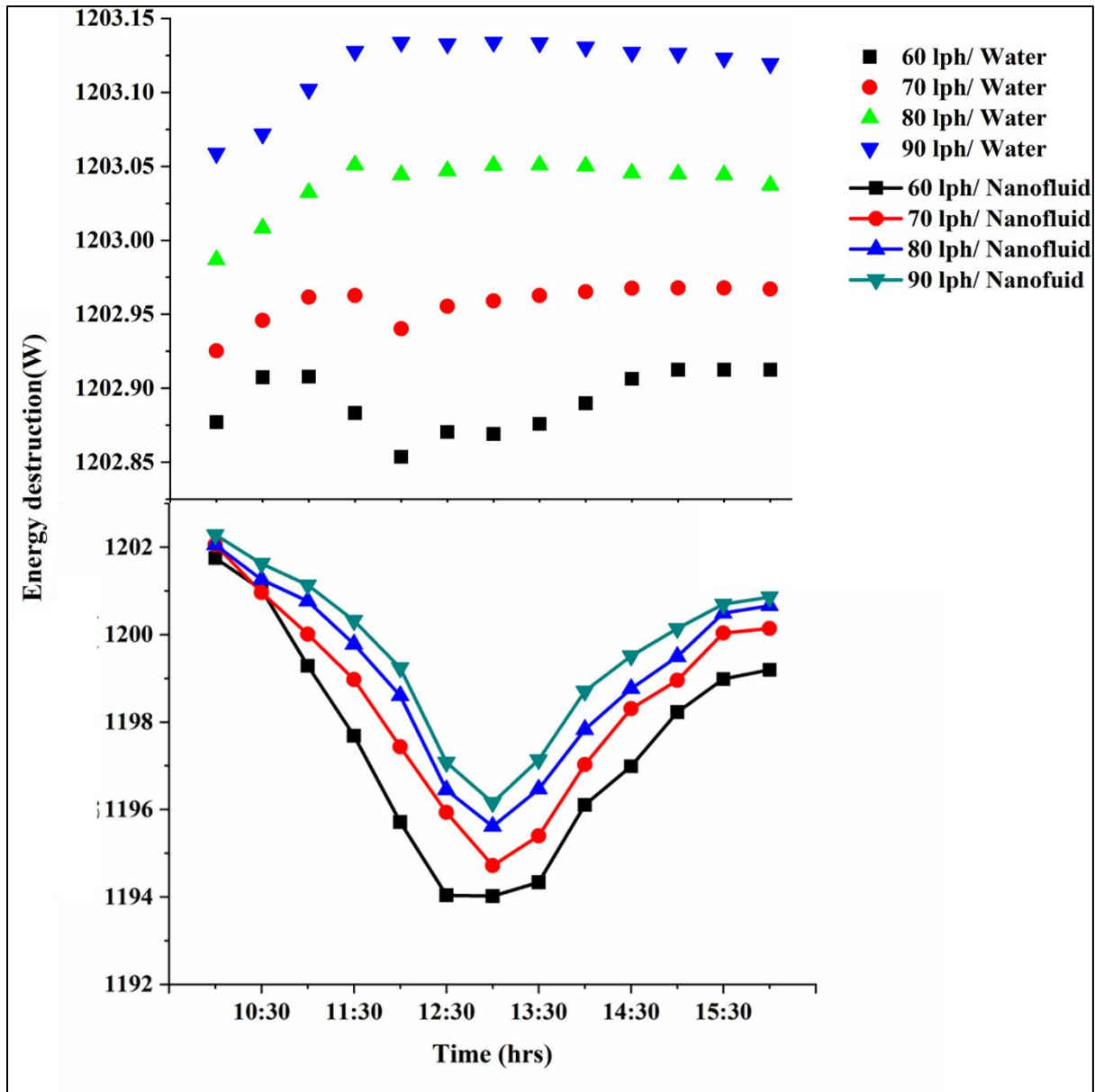
334 The thermal efficiency of the collector was estimated using the equations 3, 4, 5 and
 335 6. The transient variation of collector efficiency at various flow rate are shown in Fig. 6. The
 336 direct solar irradiance is 850 W/m^2 , which is the estimated average solar radiation at the
 337 location. The maximum thermal efficiencies for water are 13.29, 14.55, 14.96 and 15.86% at
 338 flow rates of 60, 70, 80 and 90 lph, respectively. The corresponding values of efficiencies
 339 estimated for nanofluid are 57.40, 60.41, 63.72 and 64.13% respectively. In addition, it could
 340 be observed from Fig. 6 that the maximum efficiency was obtained during the time period of
 341 12:00 pm to 2:00 pm. As mentioned before, the efficiency of the collector depends on the
 342 thermo-optical properties of the working fluid. Plasmonic SiO_2/Ag nanoparticles used in the
 343 present investigation exhibited an additional improvement in the optical absorptivity of the
 344 fluid which in turn resulted in better photo thermal conversion. It is reported that in
 345 comparison with other nanoparticles plasmonic nanoparticles exhibit an additional self-
 346 heating due to the plasmonic effect, which in turn enhance the photo thermal conversion
 347 efficiency of the nanofluid [16, 21]. The presence of CuO in the fluid transfers the absorbed

348 solar energy effectively, which is attributed to its higher thermal conductivity [17]. Reynolds
349 number is another parameter that influences the efficiency of the collector. The heat transfer
350 becomes more effective as the Reynolds number/ flow rate increases which also results in the
351 increased efficiency of the collector [25, 31]. As explained in equation (6) thermal efficiency
352 of the collector is defined as the ratio of useful heat produced to the available direct solar
353 energy. As the flow rate increases the amount of useful heat carried away by the working
354 fluid increases. As the flowrate increases the local mixing between the fluid and solid
355 particles and also between the fluid and the tube surface increases which results in enhanced
356 thermal transport and reduced thermal loss [32].



357

358 **Fig. 7.** Average entropy generation at various flowrates.

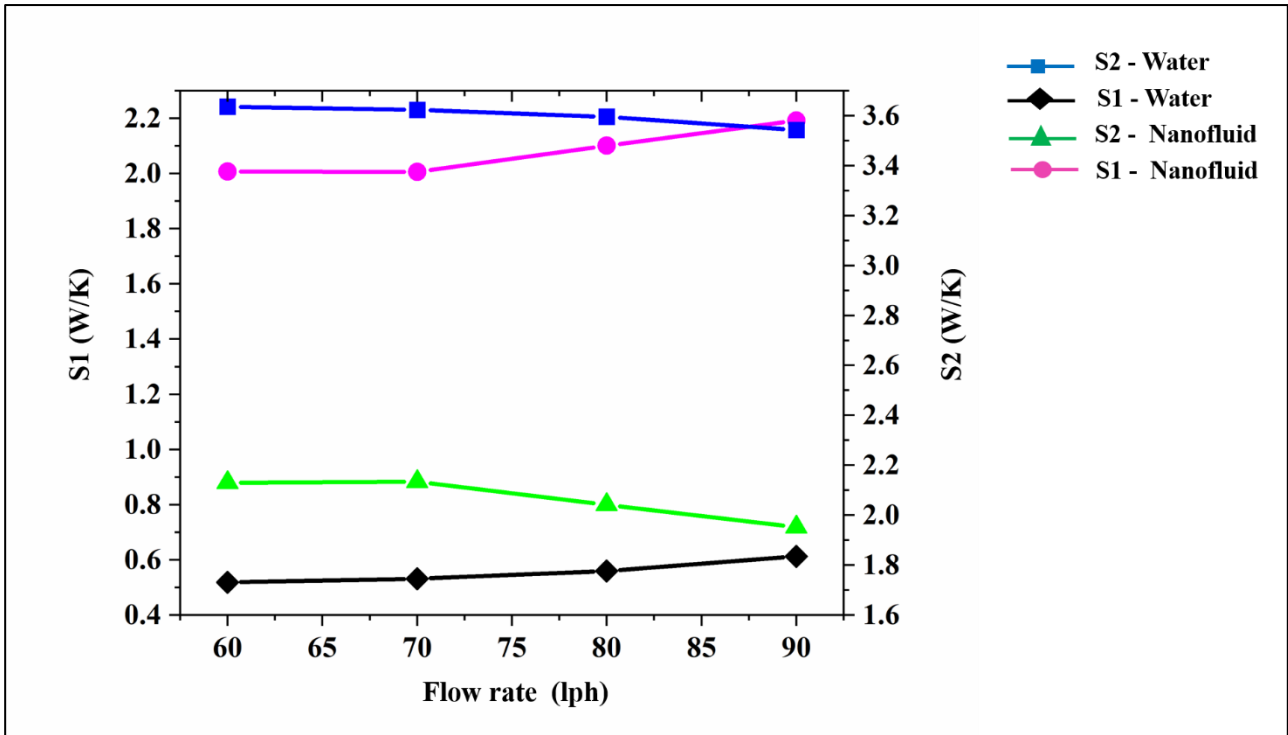


359

360 **Fig. 8.** Energy destruction profile of nanofluid and water at various flowrates.

361 Figures 7 and 8 shows the entropy generation and energy destruction calculated using
 362 equations 7, 8, 9 and 10. As can be seen from Figure 7, the entropy generation slightly
 363 decreased with the dispersion of nanoparticles in water. The entropy generation was almost
 364 constant with change in flow rate in the case of water, while it slightly increased with
 365 flowrate for nanofluid. In the present study, two factors could be accounted for the entropy
 366 generation. 1) Entropy generation due to the heat transfer from solar irradiance to the
 367 nanofluid (S1). 2) Entropy generated during to the heat loss from the nanofluid to the
 368 surroundings (S2). The contribution of the two sources (S1 & S2) to entropy generation in
 369 water and nanofluids at different flow rates is shown in Fig. 9. Among these two sources, the

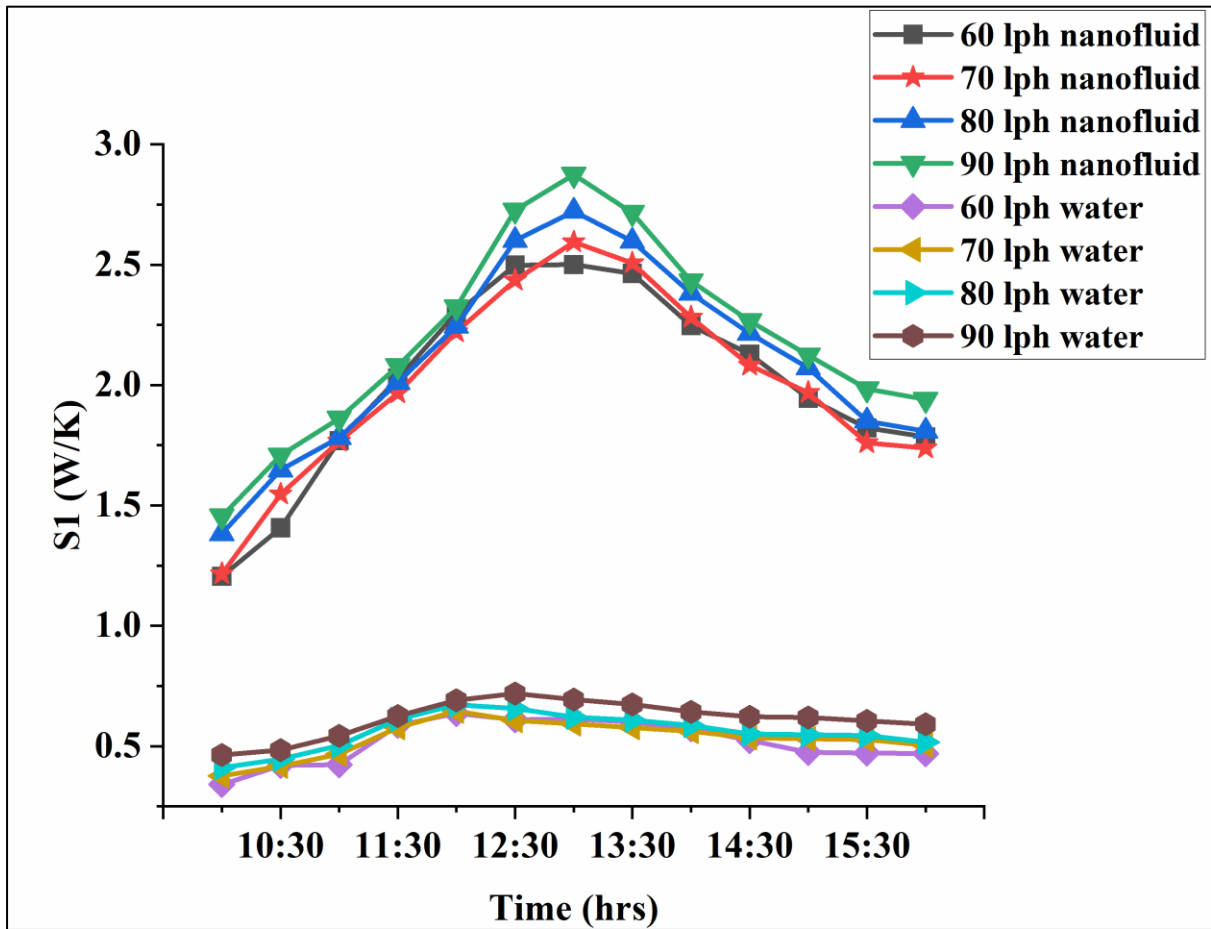
370 entropy generation due to the heating up of the nanofluid as it flows through the collector
371 tube from inlet to outlet (S_1) was found to be lesser than the entropy generation due the heat
372 losses from the nanofluid (S_2). At a flowrate of 90 lph the S_1 for water was 72.14% lower
373 than that of nanofluid. The S_1 for water was found to be less compared to nanofluid since the
374 heat gain was less in water when compared to nanofluid. However, entropy generated due to
375 the losses (S_2) was found to be less compared to water and reduces with the flow rate for
376 nanofluids. At a flowrate of 90 lph the S_2 for water is 81.54% higher than that of nanofluid.
377 The contribution of entropy generation due to heat losses (S_2) of water being much higher
378 than that of nanofluid is the reason for the slight increase in overall entropy generation
379 (S_1+S_2) of water with flow rate. On comparing figures 10 and 11 with Fig. 4 it can be seen
380 that, at a particular flow rate S_1 increases with temperature difference whereas S_2 decreases
381 (Fig 10 and 11). The higher absorption of heat by the plasmonic nanofluids results in higher
382 temperature gain of the fluid and thus contributes to S_1 . In spite of the high temperature rise
383 of the fluid the heat losses to the ambient is lesser in volumetric absorption systems
384 employing plasmonic nanofluids is evident from the decreasing S_2 values. The variation of
385 thermal efficiency and exergy efficiency with the flow rate is presented in Fig 12. It can be
386 seen that in the case of the optimised nanofluid, the exergy efficiency shows a slight decrease
387 with flow rate, while thermal efficiency increases. But the exergy efficiency of the nanofluid
388 was found to be higher than that of water with an enhancement of 9.4% at 60 lph. It could be
389 surmised that the energy losses associated with the volumetric absorption system reduces
390 with the flow rate while employing nanofluid, while the generated entropy during the gain of
391 heat from the sun increases with the flow rate. The increase in overall generation of entropy
392 is attributed to the development of temperature drop between the top wall of the collector and
393 the outlet due to the enhanced heat gain [27]. In addition, unlike the surface absorption based
394 parabolic collector, in volumetric absorption solar collector the working fluid directly absorbs
395 and convert the solar irradiance. Since the absorbing medium is in a kinematic state, the flow
396 rate directly affects the conversion of solar energy to heat. At higher flow rate of working
397 fluid, the energy conversion might be incomplete due to the insufficient time available for the
398 energy absorption owing to the rapid motion of nanoparticles in the working fluid.



399

400

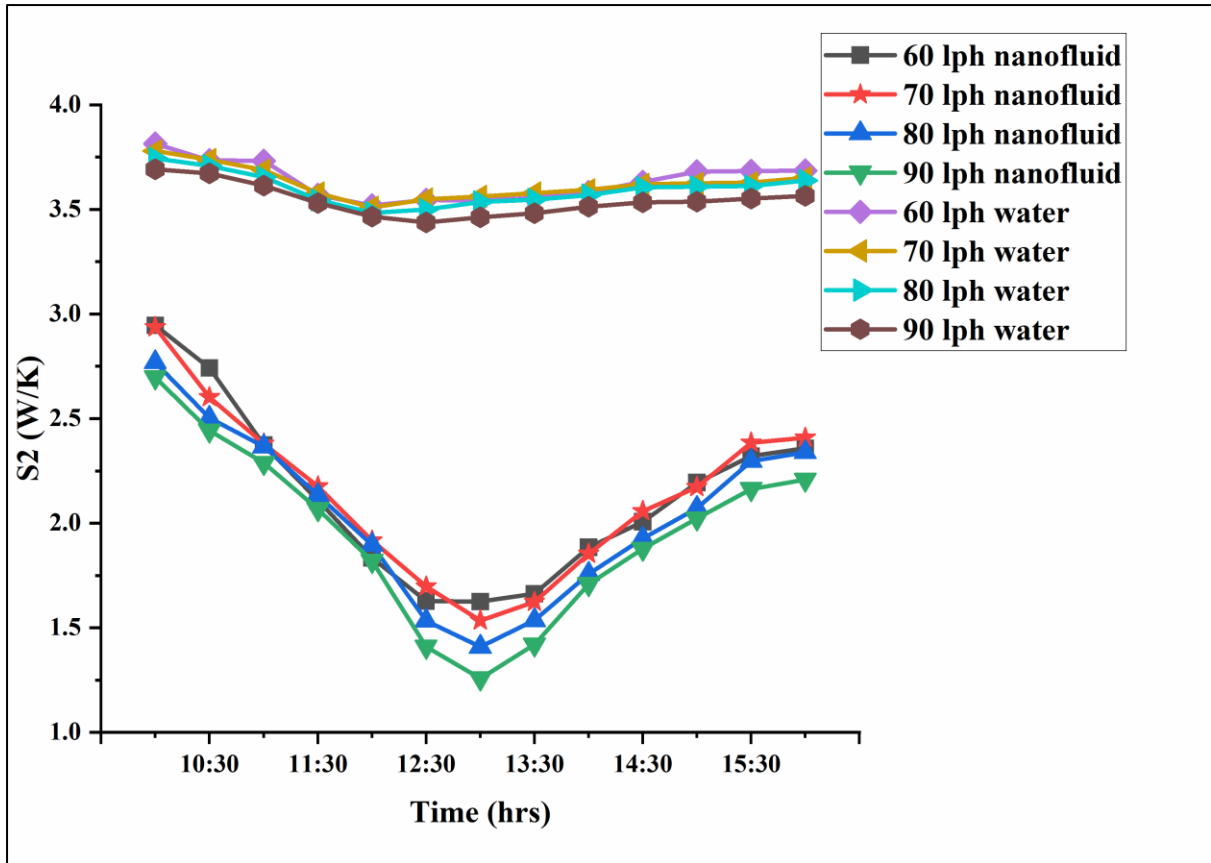
Fig. 9. Variation of average S1 and S2 with various flowrate.



401

402

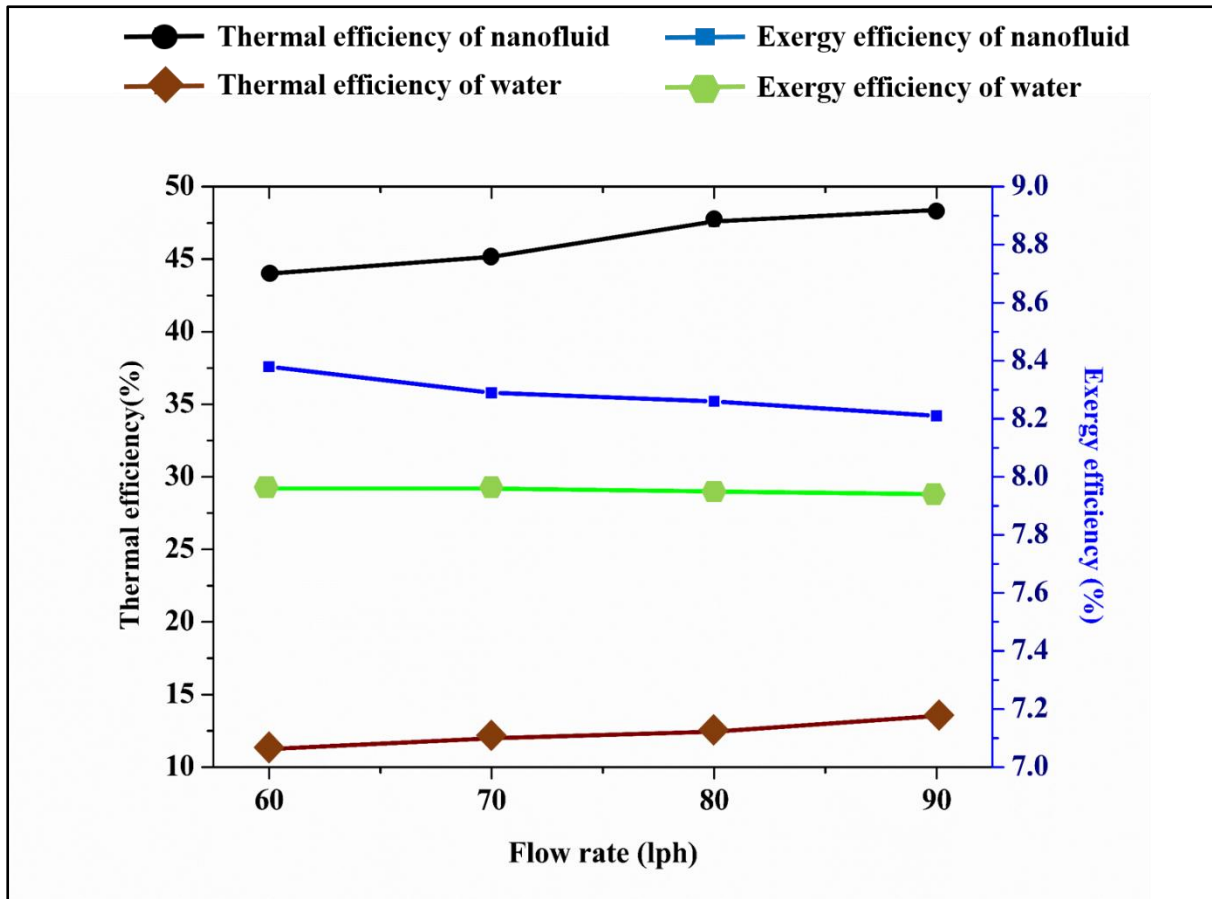
Fig.10: Instantaneous S1 of nanofluid and water at various flow rates.



403

404 **Fig. 11.** Instantaneous S2 of nanofluid and water at various flow rates.

405



406
407 **Fig. 12.** Thermal efficiency and exergy efficiency at various flowrate.

408 **Table 5. Maximum temperature difference, thermal efficiency and exergy efficiency**
409 **obtained for nanofluid and base fluid.**

Flow rate (lph)	Temperature Difference (K)		Thermal Efficiency (%)		Exergy efficiency (%)	
	Base fluid	Nanofluid	Base fluid	Nanofluid	Base Fluid	Nanofluid
60	2.71	10.8	13.80	55.01	7.97	8.64
70	2.46	10.01	14.55	59.23	7.96	8.59
80	2.21	9.06	14.96	61.34	7.95	8.52
90	2.08	8.41	15.86	64.12	7.95	8.48

410

411 **4. Conclusion**

412 The study demonstrates the favourable influence of binary SiO₂/Ag-CuO nanofluid on
413 augmenting the performance of volumetric absorption parabolic solar collector. The
414 constituents in the nanofluid was optimised using the response surface methodology and
415 desirability function. Nanofluid of optimum constituents (RTC of 1.234 and SRAF of

416 82.84%) was used as the working fluid in the volumetric absorption parabolic solar collector
417 and the effect of flow rate on various performance parameters were estimated. The major
418 findings are summarised as follows:

- 419 • A maximum temperature difference of 10.8K was observed for nanofluid at 60lph and
420 8.41K at 90 lph.
- 421 • SiO₂/Ag-CuO nanofluid improved the thermal performance of the collector with a
422 maximum overall enhancement of 48.74% in thermal efficiency noted at a flow rate
423 of 90lph.
- 424 • Increase in the flow rate leads to enhanced thermal efficiency of the collector, the
425 maximum thermal efficiency of 55.01% and 64.12% were obtained at 60lph and
426 90lph.
- 427 • The presence of SiO₂/Ag-CuO nanofluid reduced the entropy generation and thus
428 improved the exergy efficiency of the collector. However, entropy generation
429 increased with the flow rate which in turn reduced the exergy efficiency.
- 430 • Exergy efficiency of collector using nanofluid was enhanced by 8.4% at 60 lph, in
431 comparison with water.

432 REFERENCES

- [1] Sanaz Akbarzadeh, Mohammad Sadegh Valipour, Heat transfer enhancement in parabolic trough collectors: A comprehensive review, *Renew Sustain Energy Rev* 92 (2018) 198–218
<https://doi.org/10.1016/j.rser.2018.04.093>
- [2] R. Jain, R. Pitchumani, Fabrication and characterization of multiscale, fractal textured solar selective coatings, *Sol. Energy Mater. Sol Cells* 172 (2017) 213–219
<https://doi.org/10.1016/j.solmat.2017.07.009>
- [3] G.C. Bakos, Ch. Tsechelidou Solar aided power generation of a 300 MW lignite fired power plant combined with line-focus parabolic trough collectors field, *Renewable Energy* 60 (2013) 540-547
<https://doi.org/10.1016/j.renene.2013.05.024>
- [4] Jian-ping Meng, Xiao-peng Liu, Zhi-qiang Fu, Ke Zhang, Optical design of Cu/Zr_{0.2}AlN_{0.8}/ZrN/AlN/ZrN/AlN/Al₁₃₄O₆₂N₄ solar selective absorbing coatings *Sol. Energy* 146 (2017) 430–435
<https://doi.org/10.1016/j.solener.2017.03.012>
- [5] Xiaoxiao Yu, Yimin Xuan, Investigation on thermo-optical properties of CuO/Ag plasmonic nanofluids, *Solar Energy* 160 (2018) 200–207.
<https://doi.org/10.1016/j.solener.2017.12.007>
- [6] Tahereh B. Gorji, A.A. Ranjbar, A review on optical properties and application of nanofluids in direct absorption solar collectors (DASCs), *Renew Sustain Energy Rev* 72 (2017) 10–32
<https://doi.org/10.1016/j.rser.2017.01.015>

- [7] Harriet Kimptona, Domenico Andrea Cristaldia, Eugen Stulzb, Xunli Zhang, Thermal performance and physicochemical stability of silver nanoprism based nanofluids for direct solar absorption, *Sol. Energy* 199 (2020) 366–376
<https://doi.org/10.1016/j.solener.2020.02.039>
- [8] Shiva Gorjian, Hossein Ebadi , Francesco Calise , Ashish Shukla , Carlo Ingraio, A review on recent advancements in performance enhancement techniques for low-temperature solar collectors, *Energy Convers. Manage* 222 (2020) 113246
<https://doi.org/10.1016/j.enconman.2020.113246>
- [9] Caiyan Qin, Joong Bae Kim, Bong Jae Lee, Performance analysis of a direct-absorption parabolic-trough solar collector using plasmonic nanofluids, *Renewable Energy* 143 (2019) 24-33
<https://doi.org/10.1016/j.renene.2019.04.146>
- [10] Vishal Bhalla, Sachin Beejawat, Jay Doshi, Vikrant Khullar, Harjit Singh, Himanshu Tyagi, Silicone oil envelope for enhancing the performance of nanofluid based direct absorption solar collectors, *Renewable Energy* 145 (2020) 2733-2740
<https://doi.org/10.1016/j.renene.2019.08.024>
- [11] Kongxiang Wang, Yan He, Pengyu Liu, Ankang Kan, Zhiheng Zheng, Lingling Wang, Huaqing Xie, Wei Yu, Highly-efficient nanofluid-based direct absorption solar collector enhanced by reverse-irradiation for medium temperature applications, *Renewable Energy* 159 (2020) 652-662
<https://doi.org/10.1016/j.renene.2020.05.167>
- [12] Ahmet Z.Sahin, Mohammed Ayaz Uddin, Bekir S.Yilbas, AbdullahAl-Sharafi Performance enhancement of solar energy systems using nanofluids: An updated review, *Renewable Energy* 145 (2020) 1126-1148
<https://doi.org/10.1016/j.renene.2019.06.108>
- [13] Sarkar J, Ghosh P, Adil A, A review on hybrid nanofluids: recent research, development and applications, *Renew Sustain Energy Rev* 43 (2015) 164–177
<https://doi.org/10.1016/j.rser.2014.11.023>
- [14] Vishal Bhalla, Vikrant Khullar, Himanshu Tyagi, Experimental investigation of photo-thermal analysis of blended nanoparticles ($\text{Al}_2\text{O}_3/\text{Co}_3\text{O}_4$) for direct absorption solar thermal collector, *Renewable Energy* 123 (2018) 616-626
<https://doi.org/10.1016/j.renene.2018.01.042>
- [15] Nan Chen, Haiyan Ma, Yang Li, Jinhu Cheng, Canying Zhang, Daxiong Wu, Haitao Zhu. Complementary optical absorption and enhanced solar thermal conversion of CuO-ATO nanofluids, *Sol. Energy Mater. Sol Cells*. 162 (2017) 83-92
<https://doi.org/10.1016/j.solmat.2016.12.049>
- [16] Jia Zeng, Yimin Xuan, Enhanced solar thermal conversion and thermal conduction of MWCNT-SiO₂/Ag binary nanofluids, *Appl. Energy*, 212 (15) (2018), 809-819
<https://doi.org/10.1016/j.apenergy.2017.12.083>
- [17] Pawel Keblinski, Jeffrey A. Eastman, David G. Cahill, Nanofluid for thermal transport, *Mater. Today*, 8 (6) (2005) 36-44
[https://doi.org/10.1016/S1369-7021\(05\)70936-6](https://doi.org/10.1016/S1369-7021(05)70936-6)
- [18] Nor Azwadi Che Sidik, Muhammad Mahmud Jamil, Wan Mohd Arif Aziz Japar, Isa Muhammad Adamu, A review on preparation methods, stability and applications of hybrid nanofluids, *Renew Sustain Energy Rev* 80 (2017) 1112-1122
<https://doi.org/10.1016/j.rser.2017.05.221>
- [19] Mikko Makela, Experimental design and response surface methodology in energy applications: A tutorial review, *Energy Convers. Manage*, 151 (2017) 630-640.
<https://doi.org/10.1016/j.enconman.2017.09.021>

- [20] Wenlian Ye, Peng Yang, Yingwen Liu, Multi-objective thermodynamic optimization of a free piston Stirling engine using response surface methodology, *Energy Convers. Manage* 176 (2018) 147–163
<https://doi.org/10.1016/j.enconman.2018.09.011>
- [21] Sreehari Sreekumar, Albin Joseph, C.S. Sujith Kumar, Shijo Thomas, Investigation on influence of antimony tin oxide/silver nanofluid on direct absorption parabolic solar collector, *J. Clean. Prod.* 249 (2019) 119378
<https://doi.org/10.1016/j.jclepro.2019.119378>
- [22] A. Kasaeian, S. Daviran, R. D. Azarian, A. Rashidi, 2015, Performance evaluation and nanofluid using capability study of a solar parabolic trough collector, *J. Clean. Prod.* 89 (2015) 368–375.
<https://doi.org/10.1016/j.enconman.2014.09.056>.
- [23] E. Bellos, C. Tzivanidis, Thermal analysis of parabolic trough collector operating with mono and hybrid nanofluids, *Sustain. Energy Technol. Assess.* 26 (2018) 105–115.
<https://doi.org/10.1016/j.seta.2017.10.005>
- [24] T.P. Otanicar, P.E. Phelan, J. S. Golden, Optical properties of liquids for direct absorption solar thermal energy systems, *Sol. Energy* 83 (2009) 969–977.
<https://doi.org/10.1016/j.solener.2008.12.009>.
- [25] Yong Yang Gan, Hwai Chyuan Ong, Tau Chuan Ling, N.W.M. Zulkifli, Chin-Tsan Wang, Yung-Chin Yang, Thermal conductivity optimization and entropy generation analysis of titanium dioxide nanofluid in evacuated tube solar collector, *Appl. Therm. Eng.* 145 (2018) 155–164.
<https://doi.org/10.1016/j.applthermaleng.2018.09.012>
- [26] Moffat, R.J., 1985. Describing the uncertainties in the experimental results. *Exp. Therm. Fluid Sci.* 1, 3-17.
[https://doi.org/10.1016/0894-1777\(88\)90043-X](https://doi.org/10.1016/0894-1777(88)90043-X).
- [27] Salma Parvin, Rehana Nasrin, M.A. Alim, Heat transfer and entropy generation through nanofluid filled direct absorption solar collector, *Int. J. Heat Mass Transfer* 71 (2014) 386–395.
<http://dx.doi.org/10.1016/j.ijheatmasstransfer.2013.12.043>
- [28] Albin Joseph, Sreehari Sreekumar, C S Sujith kumar, Shijo Thomas, Optimisation of thermo-optical properties of SiO₂/Ag-CuO nanofluid for direct absorption solar collectors, *J. Mol. Liq.* (2019) 111986.
<https://doi.org/10.1016/j.molliq.2019.111986>
- [29] T. Aguilar, E. Sani, L. Mercatelli, I. Carrillo-Berdugo, E. Torres, J. Navas, Exfoliated graphene oxide-based nanofluids with enhanced thermal and optical properties for solar collectors in concentrating solar power, *J. Mol. Liq* 306 (2020) 112682.
<https://doi.org/10.1016/j.molliq.2020.112862>
- [30] Omid Mahian, Ali Kianifar, Soteris A. Kalogirou, Ioan Pop, Somchai Wongwises, A review of the applications of nanofluids in solar energy, *Int. J. Heat Mass Transfer* 57 (2013) 582–594
<http://dx.doi.org/10.1016/j.ijheatmasstransfer.2012.10.037>
- [31] M.M. Heyhat, M. Valizade, Sh. Abdolahzade, M. Maerefat, Thermal efficiency enhancement of direct absorption parabolic trough solar collector (DAPTSC) by using nanofluid and metal foam, *Energy* 192 (2020) 116662
<https://doi.org/10.1016/j.energy.2019.116662>
- [32] M.A. Sharafeldin, Gyula Grof, Evacuated tube solar collector performance using

CeO₂/water, nanofluid, J. Clean. Prod 185 (2018) 347-356
<https://doi.org/10.1016/j.jclepro.2018.03.054>

433

Conflicts of interest

The authors hereby declare that there has no conflict of interest

Author contributions

Use this form to specify the contribution of each author of your manuscript. A distinction is made between five types of contributions: Conceived and designed the analysis; Collected the data; Contributed data or analysis tools; Performed the analysis; Wrote the paper.

For each author of your manuscript, please indicate the types of contributions the author has made. An author may have made more than one type of contribution. Optionally, for each contribution type, you may specify the contribution of an author in more detail by providing a one-sentence statement in which the contribution is summarized. In the case of an author who contributed to performing the analysis, the author's contribution for instance could be specified in more detail as 'Performed the computer simulations', 'Performed the statistical analysis', or 'Performed the text mining analysis'.

If an author has made a contribution that is not covered by the five pre-defined contribution types, then please choose 'Other contribution' and provide a one-sentence statement summarizing the author's contribution.

Manuscript title: Energy and Exergy analysis of SiO₂/Ag-CuO plasmonic nanofluid on direct absorption parabolic solar collector

Author 1: Albin Joseph

- Conceived and designed the analysis**
Specify contribution in more detail (optional; no more than one sentence)
- Collected the data**
Specify contribution in more detail (optional; no more than one sentence)
- Contributed data or analysis tools**
Specify contribution in more detail (optional; no more than one sentence)
- Performed the analysis**
Specify contribution in more detail (optional; no more than one sentence)
- Wrote the paper**
Specify contribution in more detail (optional; no more than one sentence)
- Other contribution**
Specify contribution in more detail (required; no more than one sentence)

Author 2: Sreehari Sreekumar

- Conceived and designed the analysis**
Specify contribution in more detail (optional; no more than one sentence)
- Collected the data**
Specify contribution in more detail (optional; no more than one sentence)
- Contributed data or analysis tools**
Specify contribution in more detail (optional; no more than one sentence)
- Performed the analysis**
Specify contribution in more detail (optional; no more than one sentence)
- Wrote the paper**
Specify contribution in more detail (optional; no more than one sentence)
- Other contribution**
Specify contribution in more detail (required; no more than one sentence)

Author 3: Shijo Thomas

- Conceived and designed the analysis**
Specify contribution in more detail (optional; no more than one sentence)
- Collected the data**
Specify contribution in more detail (optional; no more than one sentence)
- Contributed data or analysis tools**
Specify contribution in more detail (optional; no more than one sentence)
- Performed the analysis**
Specify contribution in more detail (optional; no more than one sentence)
- Wrote the paper**
Specify contribution in more detail (optional; no more than one sentence)
- Other contribution**
Specify contribution in more detail (required; no more than one sentence)

Author 4: Enter author name

- Conceived and designed the analysis**
Specify contribution in more detail (optional; no more than one sentence)
- Collected the data**
Specify contribution in more detail (optional; no more than one sentence)
- Contributed data or analysis tools**
Specify contribution in more detail (optional; no more than one sentence)
- Performed the analysis**
Specify contribution in more detail (optional; no more than one sentence)
- Wrote the paper**
Specify contribution in more detail (optional; no more than one sentence)
- Other contribution**
Specify contribution in more detail (required; no more than one sentence)

Author 5: Enter author name

- Conceived and designed the analysis**
Specify contribution in more detail (optional; no more than one sentence)
- Collected the data**
Specify contribution in more detail (optional; no more than one sentence)
- Contributed data or analysis tools**
Specify contribution in more detail (optional; no more than one sentence)
- Performed the analysis**
Specify contribution in more detail (optional; no more than one sentence)
- Wrote the paper**
Specify contribution in more detail (optional; no more than one sentence)
- Other contribution**
Specify contribution in more detail (required; no more than one sentence)

Author 6: Enter author name

- Conceived and designed the analysis**
Specify contribution in more detail (optional; no more than one sentence)
- Collected the data**
Specify contribution in more detail (optional; no more than one sentence)
- Contributed data or analysis tools**
Specify contribution in more detail (optional; no more than one sentence)
- Performed the analysis**
Specify contribution in more detail (optional; no more than one sentence)
- Wrote the paper**
Specify contribution in more detail (optional; no more than one sentence)
- Other contribution**
Specify contribution in more detail (required; no more than one sentence)

Author 7: Enter author name

- Conceived and designed the analysis**
Specify contribution in more detail (optional; no more than one sentence)
- Collected the data**
Specify contribution in more detail (optional; no more than one sentence)
- Contributed data or analysis tools**
Specify contribution in more detail (optional; no more than one sentence)
- Performed the analysis**
Specify contribution in more detail (optional; no more than one sentence)
- Wrote the paper**
Specify contribution in more detail (optional; no more than one sentence)
- Other contribution**
Specify contribution in more detail (required; no more than one sentence)

Author 8: Enter author name

- Conceived and designed the analysis**
Specify contribution in more detail (optional; no more than one sentence)
- Collected the data**
Specify contribution in more detail (optional; no more than one sentence)
- Contributed data or analysis tools**
Specify contribution in more detail (optional; no more than one sentence)
- Performed the analysis**
Specify contribution in more detail (optional; no more than one sentence)
- Wrote the paper**
Specify contribution in more detail (optional; no more than one sentence)
- Other contribution**
Specify contribution in more detail (required; no more than one sentence)

Author 9: Enter author name

- Conceived and designed the analysis**
Specify contribution in more detail (optional; no more than one sentence)
- Collected the data**
Specify contribution in more detail (optional; no more than one sentence)
- Contributed data or analysis tools**
Specify contribution in more detail (optional; no more than one sentence)
- Performed the analysis**
Specify contribution in more detail (optional; no more than one sentence)
- Wrote the paper**
Specify contribution in more detail (optional; no more than one sentence)
- Other contribution**
Specify contribution in more detail (required; no more than one sentence)

Author 10: Enter author name

- Conceived and designed the analysis**
Specify contribution in more detail (optional; no more than one sentence)
- Collected the data**
Specify contribution in more detail (optional; no more than one sentence)
- Contributed data or analysis tools**
Specify contribution in more detail (optional; no more than one sentence)
- Performed the analysis**
Specify contribution in more detail (optional; no more than one sentence)
- Wrote the paper**
Specify contribution in more detail (optional; no more than one sentence)
- Other contribution**
Specify contribution in more detail (required; no more than one sentence)